## Simulation of glacial inceptions with the "green" McGill Paleoclimate Model

by

Anne-Sophie COCHELIN

Department of Atmospheric and Oceanic Sciences McGill University Montreal

A thesis submitted to the
Faculty of Graduate Studies and Research
in partial fulfillment of the requirements for the degree of
Master of Science

© Anne-Sophie COCHELIN, May 2004



Library and Archives Canada

Branch

Archives Canada Archives Canada

Published Heritage Direction du

395 Wellington Street Ottawa ON K1A 0N4 Canada Direction du Patrimoine de l'édition

395, rue Wellington Ottawa ON K1A 0N4 Canada

Bibliothèque et

Your file Votre référence ISBN: 0-494-06384-X Our file Notre référence ISBN: 0-494-06384-X

#### NOTICE:

The author has granted a non-exclusive license allowing Library and Archives Canada to reproduce, publish, archive, preserve, conserve, communicate to the public by telecommunication or on the Internet, loan, distribute and sell theses worldwide, for commercial or non-commercial purposes, in microform, paper, electronic and/or any other formats.

#### AVIS:

L'auteur a accordé une licence non exclusive permettant à la Bibliothèque et Archives Canada de reproduire, publier, archiver, sauvegarder, conserver, transmettre au public par télécommunication ou par l'Internet, prêter, distribuer et vendre des thèses partout dans le monde, à des fins commerciales ou autres, sur support microforme, papier, électronique et/ou autres formats.

The author retains copyright ownership and moral rights in this thesis. Neither the thesis nor substantial extracts from it may be printed or otherwise reproduced without the author's permission.

L'auteur conserve la propriété du droit d'auteur et des droits moraux qui protège cette thèse. Ni la thèse ni des extraits substantiels de celle-ci ne doivent être imprimés ou autrement reproduits sans son autorisation.

In compliance with the Canadian Privacy Act some supporting forms may have been removed from this thesis.

While these forms may be included in the document page count, their removal does not represent any loss of content from the thesis.

Conformément à la loi canadienne sur la protection de la vie privée, quelques formulaires secondaires ont été enlevés de cette thèse.

Bien que ces formulaires aient inclus dans la pagination, il n'y aura aucun contenu manquant.



#### **ABSTRACT**

The McGill Paleoclimate Model (MPM) was used to simulate the past and future glacial inceptions. This model of intermediate complexity was first run between 122 and 80 kyr BP (Before Present). After some parameter tuning, the MPM simulated the last glacial inception at 119 kyr BP. The recent addition of a vegetation component in the model led to an improvement of the results, especially for the ice sheet distribution over Eurasia.

The MPM was then run to simulate projections of the climate for the next 100 kyr and possibly the next glacial inception. When forced by a constant atmospheric  $CO_2$  concentration, the model predicted three possible evolutions for the ice volume: an imminent glacial inception (low  $CO_2$  levels), a glacial inception in 50 kyr (intermediate  $CO_2$  levels) or no glacial inception during the next 100 kyr ( $CO_2$  levels of 370 ppm and higher). This is mainly due to the exceptional configuration of the future variations of the summer insolation at high northern latitudes. The MPM also responded realistically to rapid  $CO_2$  changes. If a global warming episode was included at the beginning of the 100-kyr run, the evolution of the climate was slightly different and the threshold over which no glacial inception occurred was lower (300 ppm).

#### RÉSUMÉ

Le modèle de Paléoclimat de McGill (MPM) a été utilisé pour simuler les transitions interglaciaire - glaciaire, passée et future. Ce modèle de complexité intermédiaire a d'abord été utilisé pour des simulations entre -122 000 et -80 000 ans. Suite au réglage de quelques paramètres, le MPM a simulé la dernière transition interglaciaire - glaciaire il y a 119 000 ans. L'addition récente de la végétation dans le modèle a permis d'obtenir de meilleurs résultats, particulièrement pour la distribution des inlandsis en Eurasie.

Le MPM a ensuite été utilisé pour prédire le climat des 100 000 prochaines années et probablement la prochaine transition interglaciaire - glaciaire. Lorsque le MPM était forcé par une concentration atmosphérique constante en  $CO_2$ , le modèle a prédit trois évolutions possibles pour le volume de glace: une transition interglaciaire - glaciaire imminente (bas niveaux de  $CO_2$ ), une transition interglaciaire - glaciaire dans 50 000 ans (niveaux intermédiaires de  $CO_2$ ) ou pas de transition interglaciaire - glaciaire lors des 100 000 prochaines années (niveau de  $CO_2$  supérieur ou égal à 370 ppm). Ceci résulte principalement des faibles variations de l'énergie solaire reçue par la Terre en été, à hautes latitudes septentrionales, lors des 100 000 prochaines années. Le MPM a également répondu de façon réaliste à des changements rapides en  $CO_2$ . Lorsqu' un épisode de réchauffement global a été inséré au début de la simulation, le modèle a prédit une évolution légèrement différente du climat et une diminution de la valeur seuil de  $CO_2$  au-delà de laquelle aucune transition interglaciaire - glaciaire ne se produit (300 ppm).

## Contents

A	bstra	ct		ii
R	ésum	ιé		iii
Li	st of	Figur	es	vii
A	ckno	wledge	ements	x
1	Intr	roduction		1
2	$\operatorname{Th}\epsilon$	ory of	Milankovitch and glacial inception	7
	2.1	Glacia	al cycles and the interglacial - glacial transitions	7
		2.1.1	The Milankovitch theory	7
		2.1.2	Variations in astronomical parameters	9
		2.1.3	Climatic archives	11
		2.1.4	Importance of the ocean thermohaline circulation	13
	2.2	Past a	and future variations of the solar insolation	14
	2.3	Past a	and future changes in atmospheric $CO_2$ concentration	16
3	Mo	del des	scription	20
	3.1	Gener	al description of the model	20

CONTENTS

		3.1.1	Land-sea configuration	21
		3.1.2	Atmosphere	22
		3.1.3	Ocean	22
		3.1.4	Sea ice	23
		3.1.5	Land surface	23
		3.1.6	Ice sheet	24
		3.1.7	Running the model	25
	3.2	A new	parameterization of the solar energy disposition	26
	3.3	Green	ing of the MPM	29
		3.3.1	Interactions between the vegetation and the climate	29
		3.3.2	The vegetation model and improved land surface scheme used in the "green" MPM	31
4	Sim	ulatio	n of the last glacial inception	34
4	<b>Sim</b> 4.1		n of the last glacial inception	<b>34</b>
4		Earlie	<u>-</u>	
4	4.1	Earlie Objec	r model studies	34
4	4.1 4.2	Earlie Objec	r model studies	34 36
4	4.1 4.2	Earlie Objec First 1 4.3.1	r model studies	34 36 38
4	4.1 4.2	Earlie Objec First 1 4.3.1	r model studies	34 36 38 38
4	4.1 4.2	Earlie Object First 1 4.3.1 4.3.2	r model studies	34 36 38 38
4	4.1 4.2	Earlie Object First 1 4.3.1 4.3.2 4.3.3	r model studies	34 36 38 38 39 41
4	4.1 4.2	Earlie Object First 1 4.3.1 4.3.2 4.3.3 4.3.4	r model studies	344 366 388 389 411 422
4	4.1 4.2 4.3	Earlie Object First 1 4.3.1 4.3.2 4.3.3 4.3.4	r model studies	344 36 38 38 39 41 42 43

CONTENTS vi

		4.4.3	Evolution of the climate and the THC between 122 and 80 kyr BP	52
		4.4.4	A critique of the downscaled atmospheric data used in the MPM	53
5	Sim	ulation	of future climate changes	58
	5.1	Earlie	studies about long-term future climate changes	58
	5.2	Which	scenario for $CO_2$ ?	61
	5.3	Short-	term runs	62
		5.3.1	The canonical 2 x $CO_2$ experiment	62
		5.3.2	Global warming experiment with atmospheric $CO_2$ stabilized at a reduced level	65
	5.4	Long-t	erm runs for the next 100 kyr	68
		5.4.1	Constant $CO_2$ concentration	68
		5.4.2	Constant $CO_2$ concentration after an episode of global warming	73
6	Conclusions			78
	6.1	Summ	ary and conclusions	78
	6.2	Conclu	iding remarks	82
$\mathbf{R}$	efere	nces		84

## List of Figures

2.1	Long-term variations over the last 400 kyr and the next 100 kyr of the Earth's eccentricity, climatic precession, obliquity and 65°N insolation at the summer solstice (Berger, 1978)	15
3.1	Land-sea configuration for the MPM (the yellow grids correspond to Greenland).	21
3.2	Illustration of the one-layer atmospheric radiation model, from Z.Wang et al. (2004), in a cloud-free region. $r$ , $t$ and $a$ are vertically integrated atmospheric reflectivity, transmissivity and absorptivity respectively. $r_s$ is the surface albedo. In cloudy regions, the vertically integrated atmospheric reflectivity, transmissivity and absorptivity are deposited with a subscript $s$ .	27
	and absorptivity are denoted with a subscript c	21
3.3	Three feedbacks between vegetation and climate	30
4.1	Ice volume growth over North America, simulated by the MPM, with an outgoing longwave radiation (OLR) similar to Z.Wang <i>et al.</i> (2004) (blue), an increased ORL corresponding to a 10 % decrease of $k_{OLR}$ (red), and an ORL increased by a constant value of 2 W/ $m^2$ (green)	40
4.2	Ice volume growth over North America, simulated by the MPM, with the cloud optical depth (OD) as in Z.Wang <i>et al.</i> (2004) (blue), a cloud OD increased by 15 % (red), and a cloud OD increased by 30% (green)	41
4.3	Ice volume growth over North America, simulated by the MPM, with tree/grass/desert albedos similar to the BATS model (red) and with increased albedos for trees and grasses (blue) (see text below for albedo values)	42
4.4	Ice volume growth over North America, simulated by the MPM, with different permanent snow depths and fractions of liquid water converted into ice: 1 m and 60 % (light blue), 1 m and 70 % (black), 2 m and 60 % (red), 2 m and 70 % (green), and 2 m and 80 % (magenta)	44
4.5	Solar insolation at a high northern latitude in summer (left) due to Berger (1978) and Vostok-derived $CO_2$ concentration (right) due to (Barnola <i>et al.</i> , 1999), between 122 and 80 kyr BP	45

viii

4.6	Total ice volume simulated by the MPM between 122 and 80 kyr BP (top); ice volume over North America (middle) and over Eurasia (bottom) for the same run.	46
4.7	Total ice volume (bold green) simulated by the MPM between 122 kyr BP and 80 kyr BP, ice volume over North America (NA) and Eurasia (EU), and the sea-level equivalent ice volume from Lambeck and Chappell (2001)	47
4.8	Paleoclimate data from ODP Site 980 ( 55°29′N, 14°42′W, 2179 m) over the last 0.5 million years (Wang et al., 2002)	48
4.9	Ice sheet distribution simulated by the MPM between 30 and 75°N at 122 kyr BP (a), 116 kyr BP (b), 110 kyr BP (b), 100 kyr BP (d), 90 kyr BP (e), and 80 kyr BP (f)	56
4.10	Evolution of climatic variables simulated by the MPM between 122 and 80 kyr BP: (a) Annual mean global SAT, (b) maximum THC intensity in the North Atlantic, (c) SAT in January over North America at 72.5°N, and (d) SAT in January over the North Atlantic at 72.5°N	57
5.1	Atmospheric $CO_2$ concentration for the "2 x $CO_2$ experiment"	63
5.2	Time series of the changes, simulated by the MPM for the "equilibrium $2 \times CO_2$ " run, in annual mean global SAT (top left) and precipitation (top right). Time series of the evolution of the maximum THC intensity (bottom left) and mean sea ice area in the Southern Hemisphere (bottom right) for the same run	64
5.3	Atmospheric $CO_2$ concentration for the global warming experiment, inspired by the one used by Rahmstorf and Ganopolski (1999)	66
5.4	Time series of the changes in annual mean global SAT (top left) and precipitation (top right) simulated by the MPM for the global warming scenario, inspired by Rahmstorf and Ganopolski (1999). Time series of the evolution of the maximum THC intensity (bottom left) and mean sea ice area in the Southern Hemisphere (bottom right) for the same scenario	67
5.5	Solar insolation at a high northern latitude in summer, between 0 and 100 kyr AP, as calculated by Berger (1978)	69
5.6	Ice volume simulated by the MPM over the North Hemisphere for the next 100 kyr, with constant $CO_2$ scenarios ranging from 210 ppm (blue) to 370 ppm (dashed-dot black)	70
5.7	Maximum THC intensity simulated by the MPM for the next 100 kyr, with constant $CO_2$ scenarios: 210 ppm (blue), 230 ppm (magenta), 240 ppm (cyan), 250 ppm (red), 280 ppm (black), 310 ppm (yellow), 350 ppm (green) and 370 ppm (dasheddot black).	71

5.8	Atmospheric $CO_2$ concentration for the global warming episode used in the 100 kyr - experiment	73
5.9	Ice volume over the North Hemisphere simulated by the MPM for the next 100 kyr, with a global warming episode followed by a constant $CO_2$ scenario: 280 ppm (blue),290 ppm (red) and 300 ppm (green)	74
5.10	Maximum THC intensity simulated by the MPM with an initial global warming episode, followed by a constant $CO_2$ concentration of 280 ppm (blue), 290 ppm (red) and 300 ppm (green). The left panel represents the first 10 kyr of the run, the right panel represents the total 100 kyr of the run	<b>7</b> 5
5.11	Maximum THC intensity simulated by the MPM for the next 100 kyr with a constant $CO_2$ concentration of 300 ppm with an initial global warming episode (blue) or without (red)	76

First, I would like to thank my supervisor, Dr Lawrence A. Mysak. He has given me constant support and guidance during these past year. I really appreciated that he allowed me to work on future climatic changes, which represents a fascinating topic for me. I also thank him for having given me many opportunities to present my results to a large audience.

I also would like to thank Dr Zhaomin Wang. He was always available whenever I required assistance in my research. I am totally grateful for his help and his constant good mood. The inputs from the members of the ESMG (Earth System Modelling Group) have also been greatly appreciated. Thanks to Brian, Jan, Jean-François, Yi, Andres, Kate, Rebecca and Adam.

This research has been supported by funding from CFCAS and NSERC. I am thankful for this financial support. I am also grateful to the many people with whom I had very interesting and constructive discussions: Drs. André Berger, David Holland, Corinne Le Quéré, Philippe Huybrechts and Dennis Darby.

On a more personal note, I would like to thank a lot my parents and brothers for their moral support and unconditional encouragement. I am deeply grateful to Benoit for his constant support, patience and faith in me. I also thank my good friends Erin and Julie for their advice and our frequent tea breaks. A special thanks to my officemate Brian, who tolerated my music and helped me to solve my frequent computer bugs. A final thanks to my roommate Kevin, my friends in France and my McGill buddies: Andy, Jenn, Steve, William, Iriola, Lydia.

### Chapter 1

### Introduction

Climate change has attracted the interest of many scientists during the last century. Whereas some groups have analyzed paleoclimatic data from different kinds of climatic proxies, others have carried out modelling studies to simulate past or future climate changes. Their common objective was to study the evolution of the climate on either short-term or long-term time scales, and its sensitivity to different external forcings.

The evolution of the climate on a geologic time scale displays various periodic fluctuations, called climatic cycles. During the Quaternary Period, the climate oscillated between two extremes, the glacials and the interglacials, which together form glacial cycles. The glacials are very cold periods, characterized by the presence of huge ice sheets over the continents in the Northern Hemisphere. The interglacials are warmer periods. Temperatures of the four last interglacials reached at least the pre-industrial level. However, recent results from the EPICA consortium (pers. comm. with V. Masson Delmotte) show that the temperature varied with a smaller amplitude during the glacial cycles before 450 kyr BP. The interglacials between 800 and 450 kyr BP thus displayed a less pronounced warming. The alternation between cold and warm

2

periods is mainly attributed to a complex set of processes involving orbital forcing and internal processes and feedbacks in the climate system.

One of the greatest challenges in climate research is to explain these glacial cycles. During the last 900 kyr, the glacial cycles followed one another with an average periodicity of 100 kyr (Clark and Pollard, 1998). Each glacial cycle was composed of a short interglacial (~ 10 kyr), followed by an abrupt cooling and then a long glacial (~ 90 kyr), during which time there was a buildup of huge ice sheets on the Northern Hemisphere continents. The objective of this thesis is to study glacial inceptions, i.e., the transition between an interglacial and a glacial. After a glacial inception, the climate significantly cools down and ice sheets build up at high northern latitudes, over a period of a few millennia. Whereas paleoclimate data indicate when and how the last glacial inception occurred, it is still an open question as to when the next interglacial - glacial transition will happen and when the present interglacial will end.

The evolution of the future climate on a geological time scale is a topical problem. Some scientists tried to predict future climate trends over the next millennia from analogs in the records of past climate changes. From paleoclimatic evidence, the length of each of the last three interglacials was estimated at  $\sim 10$  to 12 kyr. The current interglacial, the Holocene, has already lasted 11 kyr and is the longest stable warm period recorded in Antarctica ice during the past 420 kyr. Assuming that the duration of the Holocene is similar in length to the last interglacials, we could think that its end is approaching, as was suggested in the 1970's (Kukla *et al.*, 1972). However, the present interglacial may not end as the past ones, due to (1) a different solar forcing in the future, and (2) the impact of anthropogenic activities.

In contrast to the past, today it is not possible to neglect the impact of human activities in the study of future climate changes. Although the study of climate changes is not new, the study of how human activity affects the Earth's climate has become recently a topic of great interest. Twentieth century climate has been

dominated by a nearly universal warming in almost all parts of the globe. The report of the Intergovernmental Panel on Climate Change (or IPCC; see Houghton et al. (2001)) notes an increase of the global average surface temperature over the  $20^{th}$  century of  $0.6 \pm 0.2^{\circ}C$ , with the 1990s being the warmest decade. The IPCC report also suggests that most of the warming of the last 50 years is due to the anthropogenically-forced increase of greenhouse gases ( $CO_2$ ,  $CH_4$ ,  $N_2O$  and others) in the atmosphere. The direct effect of these greenhouse gases on the global energy balance can be easily calculated (absorption of infra-red energy from the Earth's surface and re-emission back to Earth). However, the climate system is complex and contains many feedbacks. Its indirect responses to increased greenhouse gases are therefore more difficult to predict.

The fundamental question to ask is whether this strong and sudden anthropogenically-induced warming could totally disrupt the natural evolution of the climate, i.e., postpone the end of the current interglacial or even lead to a completely new climatic regime. Twelve thousand years ago, the sudden cooling period called "Younger Dryas", presumably due to the shut down of the ocean thermohaline circulation (THC), abruptly followed an initial warming episode during the last deglaciation (the Bolling-Allerod). Scientists wonder if this kind of abrupt climate change could occur again in the near future, due to a strong warming of the climate. The study of future climate changes thus requires the analysis of the possible competition between the natural forcing due to the orbital changes in the Earth relative to the Sun and the anthropogenically-induced forcing.

To study the future evolution of the climate, it is first necessary to establish how the climate system varies under natural conditions, without the contamination of the atmosphere and changes in land-surface conditions due to human activities. It is particularly interesting to simulate past climates with climate models, in order to understand the mechanisms that led to past climate changes depicted by the numerous marine, continental and glaciological records. Coupled climate models are used to try

to explain the non-linear relation between external forcings and climatic changes, which involve internal processes and feedbacks. Simulations of past climates are useful to validate a particular model's ability to simulate climates that are significantly different from the present one. Such a model can be further used to produce scenarios for future climate changes.

There are currently three categories of climate models: the three-dimensional general circulation or "comprehensive" models, the models of intermediate complexity and the simple box or "conceptual" models (Claussen *et al.*, 2002). The general circulation models, referred to as GCMs, contain as many details as possible (e.g., realistic land-sea configuration and land surface topography, fairly complete representations of atmospheric and oceanic physics and dynamics, a sophisticated land surface model and a dynamic-thermodynamic sea ice model). Because of their high level of complexity, the GCMs need much more computer time to run and are often used in "snapshot" or "time slice" studies. Other types of models are thus more useful for investigating the many feedbacks and interactions in the climate system, performing sensitivity studies, and running long-term, transient simulations, extending over thousands of years.

The box models have a low degree of complexity. Despite their many shortcomings, these models have been very useful in elucidating some fundamental concepts such as climate sensitivity and principles of predictability in the climate system. They help to understand the different feedbacks and internal processes involved in the climate system. Due to their short integration time, they are used to obtain a better understanding of long-term climate changes and paleoclimates. These simple models are not able to make specific climate predictions (Stocker and Knutti, 2003), but are used to investigate fundamental concepts about the dynamical behaviour of the climate system. These dynamical concepts must be further tested with more complex models.

Finally, the models of reduced complexity, referred to as EMICs (Earth system Models of Intermediate Complexity; see Claussen et al. (2002)), occupy an intermediate position with regard to the number of climatic processes and variables described. They involve more processes and dimensions than the simplified box models, but they are still orders of magnitude simpler than GCMs. Because EMICs are less complex than GCMs, the time of integration is considerably shorter. EMICs are thus widely employed in the analysis of a variety of climate change mechanisms and feedbacks, as well as in the assessment of future climate projections and in paleoclimate reconstructions. The McGill Paleoclimate Model, referred to as the MPM, is an EMIC which has been under development at McGill University since 1992 and is continously being improved.

The goal of this thesis is to simulate the last and next glacial inceptions with the MPM, forced by realistic solar orbital forcing, as calculated by Berger (1978). The first objective is to simulate the last glacial inception, by running the model between 122 and 80 kyr BP (Before Present). We wish to validate the ability of the MPM including a vegetation component (hereafter referred to as the "green" MPM) to simulate a glacial inception and to compare the results with paleoclimate data and results obtained with an earlier version of the MPM. The second objective is to run the model for the next 100 kyr in order to determine the time of the next glacial inception, i.e., the end of the present interglacial. The absence of a carbon cycle in the MPM will force us to use different prescribed scenarios of future atmospheric  $CO_2$  concentration. These scenarios will or will not include a global warming episode in the near future, due to the impact of human activities. We will therefore analyze the response of the model to these different external forcings.

The thesis is structured as follows. Chapter 2 reviews the theory of Milankovitch and presents some facts about glacial inception, variations in solar insolation and changes in  $CO_2$  concentration. Chapter 3 briefly describes the MPM, as a longer description can be found in the literature. In Chapter 4, some sensitivity experiments

on the new version of the MPM (which includes vegetation dynamics, among other things) are examined. The results of the simulation of the last glacial inception are then presented. Chapter 5 provides the results of short-term and long-term simulations for the future climate. The sensitivity of the MPM to a global warming episode is described for the next several centuries. The simulation of the climate of the next 100 kyr is then examined with different  $CO_2$  scenarios. Finally, the thesis conclusions are given in Chapter 6.

## Chapter 2

# Theory of Milankovitch and glacial inception

## 2.1 Glacial cycles and the interglacial - glacial transitions

#### 2.1.1 The Milankovitch theory

The incoming solar radiation received by the Earth has an annual periodic variation that creates the seasons; this seasonal cycle is mainly due to the tilt of the Earth's rotation axis. In addition, the seasonal and latitudinal distributions of this solar radiation have long-period oscillations due to slow variations in three orbital parameters (Berger and Loutre, 1996): the eccentricity, the obliquity and the climatic precession (see section 2.1.2).

The Milankovitch theory (Milankovitch, 1941), or astronomical theory of paleoclimate, suggests that a glaciation is initiated when the summer insolation at northern

high latitudes decreases substantially and reaches very low values. Milankovitch chose the evolution of June insolation at 65°N as one of the most sensitive indicators for ice sheet formation. A strong drop in the summer solar forcing at high northern latitudes prevents winter ice from melting completely during summer, and this allows the ice cover to persist from year to year. It leads to the progressive buildup of ice sheets at high northern latitudes and the consequent decrease of vegetation and increase of surface albedo. Because of the ice-albedo feedback, the summer temperature further decreases and the ice sheets' volume and area continue to increase, as does the sea ice area. During a glacial, the presence of sea ice and continental ice has strong impacts on the energy and water budgets of the climate system, e.g., through the ice-albedo feedback process and through the formation, flow and melting of ice.

Some scientists have disagreed with the Milankovitch theory. Imbrie et al. (1992, 1993) used the SPECMAP (Spectral Analysis, Mapping and Prediction Project) model to show that Northern Hemisphere summer insolation did not directly drive the buildup of northern ice sheets. They suggested that large drops in summer insolation drove instead a rapid growth of Arctic snow and sea ice. The latter resulted in changes in the deep water circulation in the North Atlantic which propagated to the Southern Hemisphere and induced changes in Antarctic sea ice cover and circumpolar ocean circulation. These changes finally led to adjustments in the atmospheric  $CO_2$  concentration that drove Northern Hemisphere ice sheet buildup.

On the other hand, Ruddiman (2003a) agreed with the Milankovitch theory, but added some new ideas about the role of the greenhouse gases in the glacial inception process. He suggested that, at first, the changes in ice volume at the 41 kyr-obliquity cycle led to a strong  $CO_2$  feedback (through changes in dust fluxes and surface water alkalinity), which amplified the buildup of ice sheets. After that, he argued that the variations of the July insolation at the 23 kyr-precession cycle directly forced the formation of ice sheets (as explained by the Milankovitch theory) and also the variations in  $CO_2$  and  $CH_4$  concentrations in the atmosphere (through alterations

in Southern Hemisphere processes and monsoons, respectively). These changes in greenhouse gas concentrations then enhanced the ice sheet buildup.

#### 2.1.2 Variations in astronomical parameters

The solar forcing at the top of the atmosphere slowly oscillates due to changes in three astronomical parameters: the eccentricity e, the obliquity  $\epsilon$  and the climatic precession  $e \sin \omega$ . The eccentricity e is a measure of the shape of the Earth's elliptical orbit around the Sun: the lower e is, the more circular the Earth's orbit. The obliquity  $\epsilon$  is the angle between the Earth's rotation axis and the perpendicular to the plane of the Earth's orbit. The climatic precession  $e \sin \omega$  is a measure of the Earth-Sun distance at the summer solstice, where  $\omega$  is the longitude of the perihelion (the position in which the Earth is closest to the Sun) measured from the moving equinox. As explained in Berger and Loutre (1996), the precession is determined by considering two factors: first, the Earth's axis of rotation wobbles like that of a spinning top and causes the North Pole to trace clockwise a circle in space, and second, the elliptical shape of the Earth's orbit is itself rotating. Finally, the equinoxes and solstices shift slowly around the Earth's orbit relative to the perihelion.

Long-term variations of these three astronomical parameters over the last few million years are obtained by solving the set of equations which govern the motion of the planets around the Sun and the motion of the Earth's axis due to the attraction of the Moon and the Sun on the equatorial bulge of the Earth. These variations can be expressed in trigonometrical form as quasi-periodic functions of time (Berger, 1978; Berger and Loutre, 1991), and they are used to calculate the temporal and latitudinal changes in insolation.

Over the past 3 million years, obliquity has varied between 22° and 25° with an average periodicity of 41 kyr. The oscillations of the precession have displayed two principal periods of  $\sim 23$  and 19 kyr, leading to an average period of 21 kyr. The eccentricity has varied between near circularity (e=0) and slight ellipticity (e=0.07) at a period of  $\sim 400$  kyr, with superimposed oscillations whose mean period is about 100 kyr (Berger and Loutre, 1996). Geologic proxy records of the variations of the solar insolation during the last 700 kyr contained oscillations with periodicities of 41, 23 and 100 kyr (Hays et al., 1976; Imbrie et al., 1992). While these variations on the 41 and 23 kyr time scales seem to be linearly linked to the variations of the obliquity and precession, the causes of the dominant 100-kyr cycle are still unclear (Ledley, 1995). The reason for this uncertainty is that the calculated insolation changes from eccentricity are too small to account for the strong 100-kyr cycles (Berger et al., 1993a). This 100-kyr periodicity cannot be related to the orbital forcing by any simple linear mechanism, but must involve some elements of internal nonlinear processes and feedbacks (Tarasov and Peltier, 1997). Past and future variations of the solar insolation will be further explained in section 2.2.

Milankovitch (1941) suggested that the conditions to enter a glaciation were a summer solstice at the aphelion (the position in which the Earth is farthest from the Sun), a high eccentricity and a low obliquity, i.e., a low seasonal contrast and a low insolation. These conditions have been verified for three of the four last glacial inceptions, i.e., during MIS (Marine Isotope Stage)-11, MIS-7 and MIS-5 (Vettoretti and Peltier, 2004). When the obliquity decreases, the energy received by the summer hemisphere also decreases, and there is less seasonal variation between summer and winter at middle and high latitudes. Vettoretti and Peltier (2004) show that the obliquity variations are dominant in determining the ice accumulation at high latitudes, as compared to the precession oscillations. A low obliquity reduces the insolation received by the high latitudes in late spring and thus delays the spring and summer snow melt, whereas an increase of the precession modifies the insolation later, i.e., in summer when some of the winter ice has already melted. However, we can see strong precessional signals in the proxy geological records of ice volume.

#### 2.1.3 Climatic archives

The climate transitions between glacials and interglacials are documented by records derived from deep sea sediments, continental deposits of flora, fauna and loess, and ice cores. An example of paleoclimate data from deep sea sediments is the 0.5 million year record from Ocean Drilling Program (ODP) Site 980 (Oppo et al., 1998; McManus et al., 1999). For aminiferal stable isotopes at this high-sedimentation site in the North Atlantic provide proxies for global ice volume, sea surface temperature (SST) and strength of the ocean thermohaline circulation (THC) (see Figure 4.8 in section 4.4.1). Paleoclimate data can also be extracted from fossil coral reefs. They indicate locally if the shorelines were raised or submerged, and therefore provide evidence for past sea level changes. As indicated in Lambeck and Chappell (2001), it is difficult to have records for the period before the last deglaciation because the advance of ice sheets during glaciations and the large sea level rise during deglaciations destroyed the corals. However, the Huon Peninsula of Papua New Guinea is located in an area of tectonic uplift, and major reefs have been uplifted up to 1000 m above the present-day sea level. Data showing fluctuations of sea level provide evidence of the changes in continental ice volume for the past 140 kyr. Finally, the study of ice cores gives access to paleoclimate time series that include local temperature and precipitation rates, moisture source conditions, wind strength and aerosol fluxes of marine, volcanic, terrestrial, cosmogenic and anthropogenic origin (Petit et al., 1999). Ice cores also provide direct records of past changes in atmospheric gas composition, thanks to the air bubbles entrapped in the ice (see the right panel of Figure 4.5). One of the most famous drilling stations is Vostok, in East Antarctica. Following the work of Jouzel et al. (1993), Petit et al. (1999) extended the Vostok ice core record so that it now covers four glacial-interglacial cycles. The ice is slightly older than 400 kyr at a depth of 3310 m. The 400-kyr record spans a period comparable to that covered by numerous oceanic and continental records.

In deep sea sediments, the proxies for climatic changes are calcareous skeletons of marine foraminiferal shells. They record the isotopic and chemical signatures of the water in which they lived, and especially the ratio  $\delta^{18}O$  between the heavy and light isotopes of oxygen, namely <sup>18</sup>O and <sup>16</sup>O. The value of this ratio is indicative of the temperature of the environment. The oceans had a high  $\delta^{18}O$  ratio at times of major glaciation, since the heavy <sup>18</sup>O more easily precipitated in the ocean, while moisture composed mostly of the lighter <sup>16</sup>O was transported poleward. High values of the  $\delta^{18}O$  ratio in the ocean thus indicate large ice sheets and low temperatures, while low ratios indicate small ice volumes and globally warm conditions (Lambeck et al., 2002). On the other hand, in the ice cores, a lower concentration of the less volatile <sup>18</sup>O is observed during cold periods. The ratio  $\delta D$  compares the ratio of the two isotopes  $^{2}H$  and  $^{1}H$  with a laboratory standard.  $\delta D$  is also a good indicator of temperature. The 400-kyr Vostok temperature record was thus reconstructed from the continuous  $\delta D$  profile measured along the core (Petit et al., 1999). Finally, benthic  $\delta^{18}O$  and  $\delta^{13}C$  records provide evidence of changes in ice volume and the strength of the THC, respectively, during a glacial cycle.

Many paleoclimate records show that much of the climate variability occurs with periodicities corresponding to that of the precession, obliquity and eccentricity of the Earth's orbit. Petit et al. (1999) showed that ice volume and temperature above Antarctica, over the last 400 kyr, displayed a very clear 100-kyr signal, characterised by long glacials and shorter warm interglacials, on which high frequencies are superposed (with periods of 41, 23 and 19 kyr). The 100-kyr signal takes the form of a saw-tooth shaped curve. The 500-kyr record from ODP (ocean drilling program) site 980 (Oppo et al., 1998; McManus et al., 1999) also displayed five large glacial cycles of  $\sim 100$  kyr periodicity.

#### 2.1.4 Importance of the ocean thermohaline circulation

As we previously mentioned, many internal processes and feedbacks of the climate system may be responsible for the amplification of the orbital forcing and the domination of the 100-kyr periodicity for glacial cycles. The importance of the ocean THC for climate variability and rapid climate changes was recognized more than 40 years ago by Stommel (1961). Since the THC is able to transport a considerable amount of heat poleward, the study of variations in its intensity and structure is of great interest for climate change studies.

The MPM has been previously run to study the response of the THC to a range of cold climates. Wang and Mysak (2000) simulated an intensified THC during a slightly cold climate (as compared to the present). However, Wang et al. (2002) showed that the THC may weaken and ultimately collapse as the cooling increases. Hence, a possible sequence of events during the last glacial was suggested. During the initiation phase, the THC first became stronger in response to cold polar temperatures and change of the hydrological cycle. This intensified THC enhanced the land-ocean thermal contrast and created an abundant moisture supply which helped to maintain and feed the buildup of ice sheets at high latitudes. However, when the volume of ice sheets reached a critical value, iceberg calving occurred (Wang and Mysak, 2001) and this triggered an increase of the freshwater discharge into the ocean at the high latitudes. Reconstructed paleoclimate data (Broecker, 1994) showed the occurrence of massive iceberg discharges known as Heinrich events (Heinrich, 1988) during extensive glaciations. The excessive freshwater discharge due to iceberg calving might have weakened or even shut down the THC, which then cooled down the polar latitudes and led to a southward advance of sea ice and a further cooling of the climate by ice-albedo feedback. Therefore, while the climate was not so cold at the initiation phase of the glacial period, an extremely cold climate was eventually established.

Wang and Mysak (2002) studied the changes in THC during the last glacial in-

ception. At the beginning of the glacial period, their results show an intensification of the THC, which would have enhanced the land-sea thermal contrast at high latitudes. This would have contributed to the rapid buildup of ice sheets. Johnson and Andrews (1979) and Peltier (1994) showed that about 50% of the maximum ice volume during the last glaciation had accumulated within the first 10 kyr of the 100-kyr glacial period, essentially due to an abundant moisture supply from the subpolar oceans.

## 2.2 Past and future variations of the solar insolation

Loutre and Berger (2000b) showed that the 100-kyr glacial-interglacial cycle in the Northern Hemisphere ice volume cannot be reproduced with their model if the solar insolation is kept constant. This result confirms the idea that the orbital forcing acted as a pacemaker for the ice ages (Hays et al., 1976) and induced feedbacks in the climate system, which amplified the direct radiative impact and generated large climatic changes (Berger et al., 1990).

Figure 2.1 shows the variations of the eccentricity, the climatic precession, the obliquity and the solar insolation in June at 65°N (Berger, 1978), between 400 kyr BP (Before Present) and 100 kyr AP (After Present). Based on the Milankovitch theory, glacial inceptions are said to occur as the solar insolation approaches sufficiently low values, which was the case at around 116 kyr BP ( $\sim 440~W/m^2$ ; see bottom panel in Figure 2.1), time of the last glacial inception. At this time, we also observe a fairly high eccentricity, a low obliquity and a high climatic precession, i.e., the summer solstice at aphelion (see Figure 2.1). The conditions were thus perfect for the initiation of a glacial period (Milankovitch, 1941).

It is not easy to determine then when the next glacial inception will occur. As

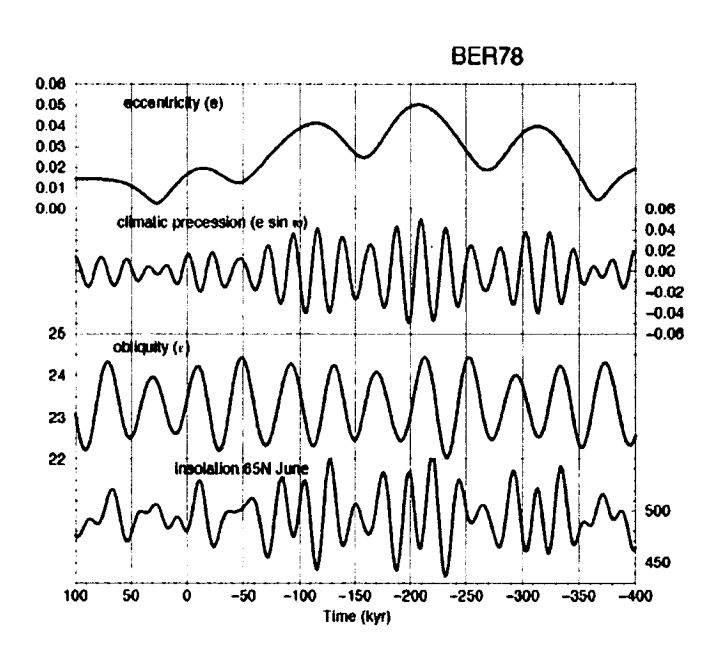


Figure 2.1: Long-term variations over the last 400 kyr and the next 100 kyr of the Earth's eccentricity, climatic precession, obliquity and 65°N insolation at the summer solstice (Berger, 1978).

explained in Berger and Loutre (1996) and shown on Figure 2.1, the eccentricity today is quite small (0.0167) and will continue to decrease, reaching almost zero (0.0027) at 27 kyr AP (Berger, 2001). The obliquity is at an intermediate value (23.45°) and decreasing. The climatic precession today has a high value ( $e \sin \omega = 0.016$ ), i.e., winter (summer) occurs presently at the perihelion (aphelion) but will occur at the aphelion (perihelion) within 10 kyr. Since the eccentricity is at present day near the end of a 400-kyr cycle, its value will be low and will vary little for the next 100 kyr. The future evolution of the climatic precession, which is proportional to the eccentricity, also displays very small-amplitude variations. Due to the exceptional configuration of the eccentricity and the fact that the daily insolation is mainly a function of precession (Berger et al., 1993a), the solar insolation will vary very little for the next 100 kyr (no more than 46  $Wm^{-2}$  in the next 100 kyr), as seen on Figure 2.1. The next minimum of the solar insolation will occur around 50 kyr AP. But this value ( $\sim 460~W/m^2$ ) is notably larger than the insolation minimum characteristic of the last three glacial inceptions. Therefore the fundamental question to ask is whether

this value will be low enough to trigger a glaciation. We shall attempt to answer this question in Chapter 5.

This exceptional future configuration of the solar insolation shown in Figure 2.1 has very few analogues in the past (Berger and Loutre, 1996). Assuming that the insolation is the main driving force for slow changes in the climate system, the best and closest analogue for our near future climate is the climate some 400 kyr BP, i.e., the MIS-11 (Loutre and Berger, 2000a; Loutre, 2003). Vettoretti and Peltier (2004) show, however, that the present-day obliquity and precession are not in phase as was the case for the glacial inception of MIS-11. The present-day orbital configuration is more similar to MIS-9 (around 320 kyr ago), even if the present-day value of obliquity and precession are two times smaller than at MIS-9.

## 2.3 Past and future changes in atmospheric $CO_2$ concentration

Vostok ice core data over the last 400 kyr show a close correlation between the temperature (as seen in the isotope ratio  $\delta D$ ) over Antarctic and the tropospheric atmospheric concentrations of  $CO_2$  and  $CH_4$  (Petit et al., 1999). This suggests that variations in the greenhouse gases may have contributed significantly to the glacial-interglacial transitions, by amplifying the orbital forcing. Simulations of the last glacial maximum by the Louvain-la-Neuve (LLN) EMIC (Berger et al., 1993b) showed that long-term  $CO_2$  changes are responsible for roughly 50% of the simulated temperature change and 30% of the ice volume change over the Northern Hemisphere.

Whether  $CO_2$  is a primary driver of glacial cycles or simply acts as a strong positive feedback is still an open question. Cuffey and Vimeux (2001) analyzed Vostok paleoclimate data after deuterium-excess correction and showed that, for the last 150

kyr, the  $CO_2$  changes followed the temperature changes with a delay of approximately 5 kyr. This lag might be due to the slow response of the ocean circulation and deepwater ventilation. Some recent studies have argued that  $CO_2$  may drive glacial cycles, if its variation coincides with a specific set of orbital configuration changes. Studying the climate of the MIS 11 ( $\sim$  400 kyr ago), Loutre (2003) showed that the climate entered rapidly into a glacial period when the insolation and the  $CO_2$  concentration decreased simultaneously or with a small time lag (5 to 9 kyr). On the other hand, if the  $CO_2$  concentration value remains high while the insolation decreases, the climate stays longer in the interglacial state. As MIS 11 is the best analogue for future climate, this relates quite well to what could happen during the next centuries to millennia, depending on how the climate system absorbs the excess of atmospheric  $CO_2$ . Finally, Vettoretti and Peltier (2004) showed that the  $CO_2$  forcing in combination with an eccentricity-precession forcing can produce the same effect as an obliquity forcing at high Northern Hemisphere latitudes. A glacial inception may therefore occur if there is a strong obliquity forcing or a combination of a  $CO_2$  forcing and an eccentricityprecession forcing.

Ruddiman and Thomson (2001) and Ruddiman (2003a) showed that the green-house gases  $CO_2$  and  $CH_4$  started to rise between 8 and 5 kyr ago, in contrast to their "natural" evolution, due to anthropogenic causes. Ruddiman and Thomson (2001) suggested that the increase of methane was due to human activities such as tending livestock, human waste production, biomass burning, and especially irrigation for rice. Ruddiman (2003b) proposed that early deforestation in Europe and Asia may be responsible for the anomalous increase in  $CO_2$  that started 8 kyr ago. This increase in methane and carbon dioxide could have been large enough to prevent a glaciation a few kyr ago, as we will see in Chapter 5.

Vostok data show that the  $CO_2$  level varied between approximately 180 and 280 ppm during the past 420 kyr. Since the Industrial Revolution, which started in the laste 1700s, the atmospheric  $CO_2$  concentration has been undergoing an exponential

increase from 280 ppm in the mid  $18^{th}$  century to around 373 ppm today. Moreover, other gases in the troposphere such as methane  $(CH_4)$ , nitrous oxide  $(N_2O)$ , water vapor  $(H_2O)$ , ozone  $(O_3)$  and halogenated species (CFCs) are reinforcing the impact of  $CO_2$  by strongly absorbing thermal radiation re-radiated into the atmosphere from the surface (Loutre, 1995). The present-day levels of  $CO_2$  are therefore unprecedented during the past 420 kyr. Moreover, the report of Houghton et al. (2001) estimates that, largely due to human activities, the future  $CO_2$  concentration may become larger than 700 ppmv over the next one to two centuries. Kump (2002) further added that the  $CO_2$  concentration may reach 2000 ppm if all the world's coal supplies are used in the next few centuries.

In addition to the anthropogenically-induced increase, the  $CO_2$  concentration in the atmosphere also varies because of complex exchanges of carbon among the ocean, atmosphere and terrestrial biomass. These natural variations in the global carbon cycle affect and are affected by climate change. During the Quaternary ice ages,  $CO_2$ was removed from the atmosphere and absorbed by the cold oceans that had a higher solubility than at present (Beerling and Woodward, 2001). During glacial periods the oceanic reservoirs are thought to have sequestered large amounts of carbon (Broecker and Peng, 1993). Carbon was then transferred to the terrestrial biosphere from the ocean via the atmosphere during the deglaciation. Global warming might lower the ability of the ocean to hold  $CO_2$ , which will leave more  $CO_2$  in the atmosphere. There are three reasons to explain this (Howard, 1997). First,  $CO_2$  is less soluble in a warm ocean. Second, as the sea level and the SST increase, calcium carbonate production and burial increase. This lowers the ocean's alkalinity and its ability to hold  $CO_2$ . Finally, the export of carbon from the surface to the deep ocean is reduced due to decreased biological production of soft tissue. Visser et al. (2003) suggested that a warming of the tropical ocean by 3.5 to 5°C may lead to a rise of the atmospheric  $CO_2$ concentration by 80 ppm. A complete account of future changes in atmospheric  $CO_2$ requires therefore a quantitative analysis of the  $CO_2$  emissions, the oceanic uptake of  $CO_2$  and the storage of carbon in vegetation and in soils.

Since most climate models do not have an interactive carbon cycle, they cannot calculate the emission and absorption of  $CO_2$  by the terrestrial biosphere and ocean and thus have to be forced by a prescribed  $CO_2$  concentration. Simulations of past climates were run with the "natural"  $CO_2$  scenario, reconstructed from Vostok ice core data (Jouzel et al., 1993). Simulations of future climates were run with a constant  $CO_2$  concentration or with a variable one, derived from the "natural"  $CO_2$  scenario of the past 130 kyr (Loutre and Berger, 2000a). Some runs also included an anthropogenically-induced global warming episode. The exceptional configuration of the future solar insolation may allow the  $CO_2$  concentration to play an important role in climate change in the long term. Berger et al. (1996) showed that the amplification of the climatic response to orbital forcing by  $CO_2$  is especially important when the amplitude of the high northern latitudes insolation change is rather small, as it will be for the next 50 kyr.

Aerosols in the atmosphere are also important for climate because some of them can offset a part of the warming due to increasing  $CO_2$  concentrations. They can have a direct or indirect radiative effect. The direct effect is due to scattering and absorption of solar radiation by the aerosol particles. Hence, the presence of aerosols induces changes in atmospheric albedo and might lead to a cooling of the climate. On the other hand, the aerosols can act as cloud condensation nuclei and modify the cloud properties. This is the indirect effect of aerosols, which is still highly uncertain. The aerosols have an atmospheric "lifetime" of a few weeks only. They do not accumulate in the atmosphere, as greenhouse gases do. If we stopped emissions, the effect of aerosols on the radiative budget would disappear quickly. Due to this short lifetime, there is a great spatial and temporal variability in aerosol concentration (Houghton et al., 2001). Global measurements are not available. That is why the majority of models (including the MPM) simulate the future climate with a fixed aerosol concentration.

### Chapter 3

## Model description

#### 3.1 General description of the model

The McGill Paleoclimate Model (referred to as the MPM) is a six-component coupled climate model, where the dependent variables are sectorially averaged across the different ocean basins and continents. The six components are the atmosphere, the ocean, the sea ice, the land surface, the vegetation and the ice sheet; they will be described later. The model contains a seasonal cycle in response to a variable solar forcing. The atmospheric, oceanic, sea ice and land surface components were first described in Wang and Mysak (2000). Wang and Mysak (2002) extended the model by adding a 2-D dynamic ice sheet model. The atmospheric component has been modified by Wang and Mysak (2002) and Z.Wang et al. (2004). Finally, the land surface component has been extended to include a dynamic global vegetation model (Y.Wang et al., 2004). The MPM is presented as an EMIC (Earth system Model of Intermediate Complexity), according to climate model terminology (Claussen et al., 2002) and has been designed for long-term climate change studies. Below are descriptions of the physical components of the model.

#### 3.1.1 Land-sea configuration

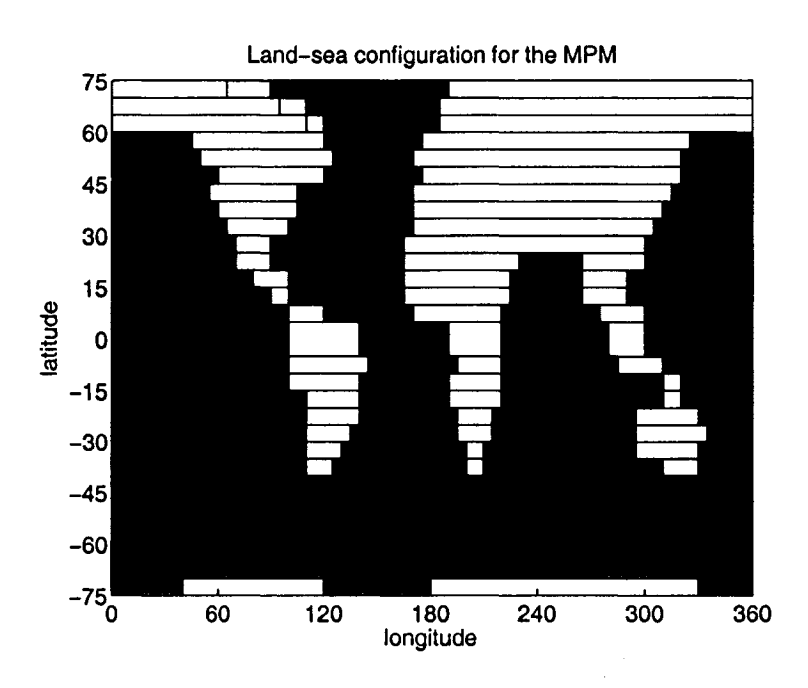


Figure 3.1: Land-sea configuration for the MPM (the yellow grids correspond to Greenland).

The land-sea configuration used in this model is shown in Figure 3.1. The model domains extends from 75°S to 75°N, with a north-south resolution of 5°, except across the equator where it is 10°. The ocean basin zonal widths vary with latitude. This configuration resolves the major continents, the three main ocean basins (Atlantic, Pacific and Indian), and the Antarctic Circumpolar Current region. The model variables are sectorially averaged across the different basins and continents. The Antarctic Circumpolar region is included as a zonally well mixed ocean. As the model domain only extends from 75°N to 75°S, the Antarctic continent and the Arctic Ocean have been omitted (Wang and Mysak, 2000). The meridional grid resolution is 5° latitude for all model components, except the ice-sheet component, which has a grid resolution of 0.5° latitude.

#### 3.1.2 Atmosphere

The atmospheric component is a sectorially averaged version of the 2-D EMBM (energy moisture balance model) of Fanning and Weaver (1996), with some extensions, as described below. The present-day monthly mean solar radiation (Berger, 1978) is prescribed at the top of the atmosphere. The heat exchanges between the atmosphere and the underlying surface are in the form of longwave radiation, shortwave radiation, latent heat and sensible heat. The radiation scheme is quite simple in Wang and Mysak (2000), however, and was improved by Z.Wang et al. (2004), who included a new solar energy disposition in the model. This will be explained in section 3.2 below.

The meridional heat and moisture transports are parameterized by a combination of advection and diffusion processes. The zonal heat transport is parameterized only as a diffusion process, and the zonal moisture transport is parameterized so that the ocean always supplies moisture to the land, in all seasons. Precipitation occurs as soon as the relative humidity exceeds a critical value. Wang and Mysak (2002) extended the MPM by employing the outgoing longwave radiation parameterization from Thompson and Warren (1982), and hence the water vapor - temperature feedback was included in the model. Wang and Mysak (2002) also downscaled the variables of surface air temperature (SAT) and precipitation over North America and Eurasia (between 30 and 75° N). In each 5° latitude band, they replace the sectorially averaged value by a set of values every 5° of longitude. Cloud and aerosols are included in the model and prescribed at the present-day observations. We will see in section 3.2 how they affect the radiation scheme.

#### 3.1.3 Ocean

The oceanic model used here is described in Stocker et al. (1992) and Bjornsson et al. (1997), and is an extension of the one-basin model of Wright and Stocker (1991).

Zonally averaged advection-diffusion equations for temperature and salinity are employed to predict their time evolution. The velocity components are diagnosed from the zonally averaged momentum equations and the continuity equation (Wright and Stocker, 1991). The equation of state is nonlinear (Wright, 1997) and the convective adjustment is taken from Schmidt and Mysak (1996). The meridional overturning streamfunction is diagnosed from the velocity components. Monthly mean wind stress from Hellerman and Rosenstein (1983) is applied to the top layer of the model. The zonally averaged east-west pressure gradient is parameterized in terms of the meridional pressure gradient (Wright and Stocker, 1991).

#### **3.1.4** Sea ice

The sea ice component is a zero-layer thermodynamic sea ice model with prescribed advection. Snow cover is not included. The ice surface temperature and the mean thickness are calculated based on Semtner (1976) and the ice concentration is predicted using the method of Hibler (1979). The meridional advection velocity of sea ice (for Northern Hemisphere only) is prescribed as in Harvey (1988). However, we know that, in a zonally averaged model, sea ice cannot be simulated accurately, especially in northern high latitudes where the spatial inhomogeneity is substantial.

#### 3.1.5 Land surface

Initially, the land surface was simply considered as either snow-free or snow-covered. Y.Wang et al. (2004) added an interactive vegetation component, which will be described in section 3.3. That is why the model is referred to as the "green" MPM. The heat capacity of the snow-free land surface is assumed to be equivalent to a water depth of 2 m (Ledley, 1991), while the heat capacity of snow over land is neglected. The snow may accumulate if there is snowfall and if the land surface temperature

falls to the freezing point. The heat capacity has been increased in regions where there are large areas of water, such as the Great Lakes region, or the Hudson Bay.

The hydrological cycle (soil moisture and runoff) for snow-free land and snow-covered land is simulated using the classic bucket model (Manabe, 1969), with a bucket depth of 15 cm. The amount of water in the bucket is calculated from melted snow, rainfall and evaporation. The surface specific humidity has been downscaled by Wang and Mysak (2002) in order to get its values in every 5° of longitude over North America and Eurasia. In the "green" MPM used in this thesis, which includes the vegetation component, the treatment of the land surface hydrological cycle remains unchanged. However, this shortcoming will be addressed in a future study by Y.Wang.

#### 3.1.6 Ice sheet

Wang and Mysak (2002) incorporated into the MPM the 2-D (latitude-longitude) dynamic ice sheet model of Marshall and Clarke (1997), with a latitude-longitude resolution of 0.5° x 0.5°. The surface air temperature, precipitation and surface specific humidity have been downscaled in order to get their values in every 5° of longitude over North America and Eurasia, from 30 to 75° N (Wang and Mysak, 2002). Snow accumulation is calculated over this 5° x 5° grid and is then linearly interpolated onto the ice sheet fine resolution grid of 0.5° x 0.5°.

The MPM neglects ice sheet thermodynamics, and hence assumes the ice sheet to be isothermal (T = -5°C). The elevation effect of orography and the freezing of rain/refreezing of meltwater are taken into account in the ice sheet growth calculation. The SAT over the ice sheet is adjusted to take into account the ice sheet height. If this temperature exceeds the melting point, ablation occurs and energy is used to melt the ice. If the SAT is below the melting point, the net snow accumulation is calculated by taking into consideration the ice sheet elevation - SAT feedback, and

by assuming that the snow is converted to ice instantaneously.

The Greenland ice sheet is located in the western half of the northern North Atlantic, as a part of the ice sheet component, whereas it is attached to the Northern American continent for the other components of the model. In Figure 3.1., the yellow grids correspond to where Greenland is attached to North America, i.e., as it is for all components of the model except the ice sheet component. The topography of Greenland has been improved by using data from P. Huybrechts (pers. comm., 2004). Thanks to a kriging process, we could adapt his 20 km x 20 km dataset to our 0.5° x 0.5° grid. Finally, the SAT over Greenland is uniformly decreased by 2°C to create cold conditions and allow the formation of the Greenland ice sheet. Letreguilly et al. (1991b) suggested that the Greenland ice sheet may have been slightly smaller at 130 kyr than at present. Cuffey and Marshall (2000) also pointed out that there was a significant reduction of the Greenland ice sheet during the Eemian, leading to a global sea level rise of 4 to 5.5 m. However, due to the coarse resolution of the MPM over Greenland, we used the present-day Greenland as an initial condition for the simulation of the last glacial inception.

In our model, ice sheets affect the climate through the thermal effect and the freshwater reservoir/release effect. First, an ice sheet can cool down the climate through the ice-albedo feedback and the absorption of latent heat when ice melts. Then, the abrupt release of freshwater from melting ice sheets to the ocean may significantly change the THC through a reduction in NADW formation, and hence affect other climate system quantities such as SST, SAT, etc.

#### 3.1.7 Running the model

The atmosphere, land surface and sea ice models have a time step of 6 h; it is 15 days for the ocean and 20 years for the ice sheet model. The atmosphere, land surface, sea

ice and ice sheet models are first spun up together, for 300 years, to reach an equilibrium, under the forcing of monthly mean solar radiation at the top of the atmosphere of Berger (1978), and the zonally averaged monthly mean SST (Levitus, 1982). The ocean model is then spun up for 5000 years by restoring the mixed layer temperature and salinity to their observed zonally averaged surface monthly mean values (Levitus, 1982). After the equilibrium states are obtained, the ocean component is coupled to the other components using flux adjustments (Manabe and Stouffer, 1988, 1994; Gordon and O'Farrell, 1997). The coupled model is then integrated for tens of thousands of years.

## 3.2 A new parameterization of the solar energy disposition

Wang and Mysak (2000) calculated the solar insolation absorbed by the atmosphere as

$$Q_{SSW}(1-\alpha_A)(1-a)(1+aB)$$

where  $Q_{SSW}$  is the monthly mean solar insolation at the TOA (Berger, 1978),  $\alpha_A$  is the atmospheric albedo, that takes into account the reflection processes due to clouds, aerosols, water vapor,  $CO_2$  and other gases, a is the atmospheric transmissivity of solar radiation, and B is the surface albedo. The determination of the zonally averaged atmospheric albedo is arbitrary, and the total solar insolation absorbed by the atmosphere is probably too large over regions with high surface albedo.

Z.Wang et al. (2004) modified the solar energy disposition (SED) in order to describe accurately the physical mechanisms of radiative processes and to take into account more accurately the properties of the ground and atmosphere. Z.Wang et al. (2004) thus developed a rigorous solar radiation scheme, suitable for EMBMs, and used it together with present-day climatological data for clouds, aerosols, precipitable

water and surface albedo in order to derive the SED in the climate system.

The SED into the atmosphere, at the surface and that escaped to space are first expressed as functions of the surface albedo,  $r_s$ , and the integrated atmospheric reflectivity, transmissivity, absorptivity and cloud amount for a one-layer atmosphere which includes a cloud region and aerosols. The integrated atmospheric reflectivity, transmissivity and absorptivity for the whole atmospheric column are r, t and a respectively for any clear sky region, and  $r_c$ ,  $t_c$  and  $a_c$  respectively for any cloudy region. Multiple reflections between the atmospheric layer and the surface are assumed, as shown on Figure 3.2.

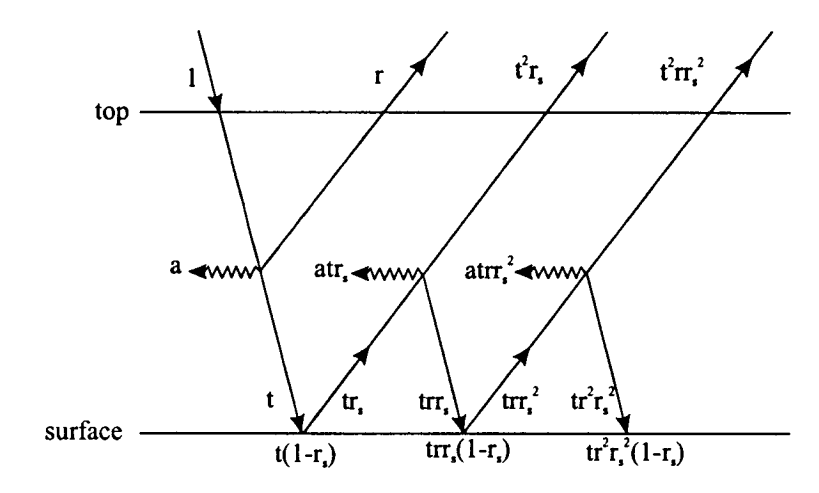


Figure 3.2: Illustration of the one-layer atmospheric radiation model, from Z.Wang et al. (2004), in a cloud-free region. r, t and a are vertically integrated atmospheric reflectivity, transmissivity and absorptivity respectively.  $r_s$  is the surface albedo. In cloudy regions, the vertically integrated atmospheric reflectivity, transmissivity and absorptivity are denoted with a subscript c.

As explained in Z. Wang et al. (2004), the disposition of unit incident solar insolation into the atmosphere,  $Q_a$ , is given by

$$Q_a = (1 - A_c)(a + \frac{atr_s}{1 - rr_s}) + A_c(a_c + \frac{a_c t_c r_s}{1 - r_c r_s})$$

where  $A_c$  is the cloud amount. Similarly, the disposition of unit incident solar insolation at the surface,  $Q_s$ , is given by

$$Q_s = (1 - A_c) \frac{t(1 - r_s)}{1 - rr_s} + A_c \frac{t_c(1 - r_s)}{1 - r_c r_s},$$

and the disposition of unit incident solar insolation that escapes to space,  $Q_e$ , is given by

$$Q_e = (1 - A_c)(r + \frac{t^2 r_s}{1 - r r_s}) + A_c(r_c + \frac{t_c^2 r_s}{1 - r_c r_s}).$$

Since r+t+a=1 and  $r_c+t_c+a_c=1$ , we note that  $Q_a+Q_s+Q_e=1$ .

An atmospheric radiative-convective model (RCM) is then used to parameterize the integrated atmospheric reflectivity and transmissivity (for clear and cloudy skies) in terms of cloud optical depth, aerosol optical depth, precipitable water, and solar zenith angle. The atmospheric reflectivity and transmissivity are decomposed into their climatological values (multi-year global annual means with solar zenith angle at 60°) plus perturbations caused by variations of atmospheric compositions which are functions of space, time and solar zenith angle. The perturbations caused by clouds, aerosols and precipitable water are taken into account; the perturbations caused by  $CO_2$  and ozone are neglected since they are very small. Sensitivity experiments done by Z. Wang et al. (2004) show that variations in cloud optical depths have a strong influence on the reflectivity and transmissivity of the atmosphere, but little effect on the atmospheric absorption. Aerosol optical depth modifications lead to a relatively large change of the atmospheric absorption, in addition to fluctuations of the energy flux escaped to space and that absorbed at the surface. Surface albedo changes lead to changes of the top of the atmosphere escaped energy flux, atmospheric absorption and surface absorption. Z. Wang et al. (2004) finally showed that the calculated SEDs are in good agreement with the satellite derived data (Li and Leighton, 1993; Gupta et al., 1999). We can thus use the method proposed by Z. Wang et al. (2004) to derive the present-day climatology of SED by using the climatological data of cloud amount and optical depth, precipitable water, aerosol optical depth and surface albedo.

In the MPM, the atmosphere component is an EMBM. The cloud amount, cloud optical depth and aerosol optical depths are obtained from present-day observational data and are fixed in the model; precipitable water is calculated by the model, ac-

cording to SAT. Cloud amount is obtained from three independent data sources. The cloud optical depth observed data contain a 30 % uncertainty. It is thus quite common to tune the modelled cloud optical depth in order to get a more realistic solar energy flux escaped to space.

#### 3.3 Greening of the MPM

#### 3.3.1 Interactions between the vegetation and the climate

Since vegetation and climate interact continually, it is necessary to incorporate a dynamic vegetation model into a physical climate model if we want to simulate the climate accurately. However, the representation of vegetation in climate models is usually limited because vegetation is highly heterogeneous. Furthermore, terrestrial vegetation interacts with the global climate over a wide range of time scales, through the exchange of energy, water,  $CO_2$  and other trace constituents (Aber, 1992). This makes the incorporation of terrestrial vegetation into climate models very challenging.

On the one hand, vegetation has a great impact on climate, as shown by the three feedbacks that include vegetation (Figure 3.3). It has an impact on the global energy cycle through land-surface processes. It changes the surface albedo and thus the energy absorbed by the surface, as well as it modifies the amounts of latent and sensible heat exchanged between the Earth's surface and the atmosphere. It also modifies the hydrological cycle, through rainfall interception by the canopy, evapotranspiration from the vegetation (about 20% of the water added to the atmosphere annually comes from evapotranspiration), regulation of atmospheric humidity, and modification of the surface roughness. Finally, the terrestrial biosphere, i.e., the living biomass and the soils, is the second major carbon reservoir of the Earth system (2100 Gt); the global carbon cycle and terrestrial vegetation are thus linked through

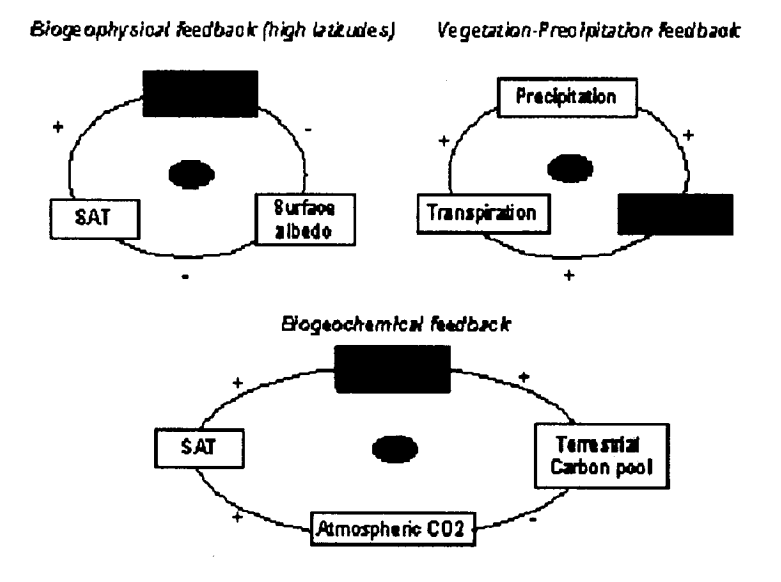


Figure 3.3: Three feedbacks between vegetation and climate.

the vegetation seasonal cycle and also through long-term variability associated with natural and anthropogenic changes in atmospheric  $CO_2$  concentration.

On the other hand, climate has also an impact on vegetation, through variations of the solar insolation. Changes in temperature have been the primary cause for the movement of vegetation zones, for example during ice buildup or ice retreat.

A good vegetation model to be incorporated into a climate model is one that is interactive, whereby vegetation patterns can influence and be influenced by the climate. "Dynamic Global Vegetation Models" (DGVMs) have a vegetation interactive component and allow climate - vegetation feedbacks. All DVGMs treat vegetation cover as a fractional representation consisting of different plant function types.

Y.Wang et al. (2004) therefore incorporated certain aspects of the terrestrial biosphere into the MPM, by including vegetation dynamics and improving the land surface scheme. These changes for the MPM are now described below.

### 3.3.2 The vegetation model and improved land surface scheme used in the "green" MPM

The DGVM used in the MPM is VECODE (VEgetation COntinuous DEscription), which has been developed by Brovkin *et al.* (1997) for EMIC-type climate models. Although many processes are missing in VECODE (e.g., evapotranspiration, water balance, canopy temperature, etc), it is a suitable vegetation model for long-term climate studies using intermediate complexity climate models. Vegetation is classified into two main types - trees and grasses; the rest is desert.

VECODE is first coupled with the reduced MPM (i.e., the atmosphere, land surface and sea ice components). Since vegetation evolves on longer time scales than the atmospheric component in the climate system, different timesteps are used (1 year for VECODE, 6 hours for the rest of the reduced MPM). The computed annual precipitation, annual and monthly mean surface air temperatures and annual mean soil moisture content from the reduced MPM are used to force VECODE and to produce a vegetation cover for the corresponding climate. Then, the impact of this vegetation on the climate is taken into account by the effects that vegetation has on the surface albedo and roughness.

In order to incorporate this vegetation model into the physical climate model, a new land surface scheme, which includes VECODE, was introduced into the MPM. It is adapted from BATS (Biosphere-Atmosphere Transfer Scheme) (Dickinson et al., 1986, 1993). It focuses on the influence on climate of the energy exchanges between the land surface and the atmosphere. The two major improvements to the MPM resulting from this new land surface scheme are the parameterization of the seasonal cycle of terrestrial vegetation, and the calculation of a seasonal land surface albedo by using vegetation-related parameters, snow depth and the model's climatology. Furthermore, this new land surface scheme also incorporated the parameterization of

deciduous and evergreen forests (characterized by a different leaf area index), using the model's climatology and the VECODE model. In extratropical regions, the forests can be well mixed (i.e., a combination of evergreen and deciduous forests), while all trees are supposed to be mainly evergreen trees at tropical latitudes.

In this new land surface scheme, the land surface energy budget calculation is in terms of surface albedo, which takes into account soil moisture, vegetation cover and snow cover, including the effective snow cover when vegetation is present. The snow-free albedo is written as follows:

$$\alpha_{S_{free}} = f_t \alpha_t + f_g \alpha_g + f_d \alpha_d$$

where  $f_t$ ,  $f_g$  and  $f_d$  are the fractions of trees, grasses and deserts given by VECODE, and  $\alpha_t$ ,  $\alpha_g$  and  $\alpha_d$  are the integrated albedos for trees, grasses and deserts. The snow-covered albedo is written in terms of the weighted albedo of snow-free and snow-covered land surfaces. Calculations of these albedos are explained in detail in Y.Wang et al. (2004). The model performance might be influenced by the parameters chosen to describe the vegetation (tree/grass/desert albedos) and by the resolution of the model.

The results cited in Y.Wang et al. (2004) show considerable improvement of the model's simulation of the present-day climate as compared with that simulated in the original physically-based MPM. In particular, the strong seasonality of terrestrial vegetation and the associated land surface albedo variation are in good agreement with several satellite observations. The zonal distribution of annual mean precipitation is now significantly improved in the green MPM, especially in the NH middle and high latitudes. However, the simulated SAT is still too high in the northern subtropical and high-latitude regions. The reasons for this bias are probably because of the absence of (a) atmospheric dynamics (which controls the transports of heat and moisture) and (b) the Arctic Ocean. The next objective of this thesis, described further below in Chapter 4, will be to test the ability of the green MPM to simulate

the last glacial inception.

However, an understanding of all the mechanisms that control the distribution of different vegetation types is still unclear. The importance and uncertainty about the strength of the feedbacks of vegetation on climate therefore indicate a need for further investigation. The model is able to calculate the carbon storage in the green biomass, structural biomass, fast soil organic material and slow soil organic material. However, it is not able to calculate the atmospheric  $CO_2$  concentration and the amount of carbon stored in the ocean. We have to prescribe the atmospheric  $CO_2$  concentration, which runs the risk there is an intrinsic inconsistency between the modelled surface vegetation, the carbon-holding capacity of the ocean and the prescribed carbon content of the atmosphere. It will therefore be interesting to include later in the MPM the terrestrial and oceanic carbon cycle in order to study in detail the role of biogeochemical feedbacks.

#### Chapter 4

# Simulation of the last glacial inception

#### 4.1 Earlier model studies

Many model studies have been directed toward investigating the 100-kyr glacial-interglacial cycles that occurred during the last 900 kyr (Clark and Pollard, 1998). These studies tried to simulate the successive glacial inceptions and terminations, as a response to changes in the summer insolation and the consequent internal climatic feedbacks. Our goal in this chapter is to simulate with the "green" MPM the last glacial inception, i.e., the interglacial to glacial transition that occurred circa 119 kyr BP, and the subsequent buildup of huge ice sheets over North America and Eurasia during the glacial period.

Vettoretti and Peltier (2004) wrote an interesting review of the work of three types of modelling groups that studied the glacial-interglacial cycles. The first group used simple models, e.g., an atmospheric energy-moisture balance model including

the influence of the ice-albedo feedback coupled to a model of global glaciology and a model of glacial isostatic adjustment (Deblonde and Peltier, 1991a,b, 1993; Tarasov and Peltier, 1997, 1999, 2004). Due to the simplicity of the models, very long simulations could be run that modelled the climate of many successive 100-kyr glacial cycles.

The second modelling group used EMICs to perform a large number of sensitivity studies and investigate the role of various feedback mechanisms in the climate system. Wang and Mysak (2000) used an earlier version of the MPM to demonstrate how the gradual cooling of high latitudes led to the intensification of the Atlantic thermohaline circulation. This might have enhanced snowfall at northern high latitudes, promoting the glacial inception. Crucifix and Loutre (2002) simulated the last interglacial with the EMIC MoBidiC and showed that the temperature-albedo feedback and the growth of summer sea ice enhanced the recession of the tundra-taiga transition zone, and therefore the glacial inception. Khodri et al. (2003) studied the role of the freshwater budget in the Arctic Ocean and demonstrated with the EMIC CLIMBER-2 that the transition between the marine isotope stage (MIS) 5e and 5d was very sensitive to the high-latitude moisture budget. Finally, Meissner et al. (2003) investigated the role of land surface dynamics with another model of intermediate complexity.

Finally, some climate simulations of the last glacial inception have also been conducted with coupled Atmosphere-Ocean models (AOGCMs). Due to the complexity of some of these GCMs, the simulations could not be run for very long times, and the glacial inception was thus simulated in a "snapshot" mode with the summer solar forcing fixed at the post-Eemian minimum (see Vettoretti and Peltier (2003a) for a detailed review). Gallimore and Kutzbach (1996) used the R15 NCAR CCM1 to perform sensitivity experiments and study the influence of vegetation on the glacial inception process. Their simulations produced a perennial snow cover only when the "tundrataiga" feedback is included in the model. Using the LMD 5.3 model, de Noblet *et al.* (1996) showed also that the orbital forcing was not sufficient to initiate glaciation,

and that the interaction with vegetation was necessary. Khodri et al. (2001) used a fully coupled AOGCM to demonstrate that ocean feedbacks might play an important role in glacial inception by cooling high latitudes and increasing the atmospheric poleward moisture transport. Using simulations with the CCCma AGCM2 in which the atmospheric  $CO_2$  concentration follows the Vostok-derived data, Vettoretti and Peltier (2003a) showed that a perennial snow cover developed at high northern latitudes solely as a consequence of orbital forcing. They suggested that many feedback mechanisms might be important for the enhancement of perennial snow cover, such as the feedback between cold climates and increased northward moisture transport.

#### 4.2 Objectives of the new experiment

Wang and Mysak (2002) ran the earlier geophysical version of the MPM between 122 and 110 kyr BP, under Milankovitch forcing, i.e., variable solar insolation calculated according to Berger (1978), and Vostok-derived atmospheric  $CO_2$  levels (Barnola et al., 1999). They simulated the last glacial inception, and the ice sheet growth over northern hemisphere high latitudes that occurred during MIS-5e/5d transition. Wang and Mysak (2002) showed the necessity of using the elevation effect of orography and a parameterization describing the freezing of rainfall and the refreezing of melted snow over an ice sheet. Because of these features and an active ocean component, they produced a rapid ice sheet growth between 120 and 110 kyr BP. The ice volume-equivalent drop in sea level during the period 122-110 kyr BP modelled by Wang and Mysak (2002) was somewhat low as compared to sea-level reconstructions. At 110 kyr BP, the total simulated ice volume reached approximately 13 x  $10^6 km^3$ , whereas the reconstructed values from paleoclimate proxy data (Lambeck and Chappell, 2001) give a volume of 20 to  $28 \times 10^6 km^3$ .

After the publication of Wang and Mysak (2002), the MPM has been further

improved. As explained in the sections 3.2 and 3.3, the two major improvements are the addition of a new solar energy disposition (SED) and a vegetation component. Our ultimate goal is to do the same transient experiment as in Wang and Mysak (2002) with the new version of the model but for a longer time period, up to 80 kyr BP. Hence with this longer run (from 122 to 80 kyr BP) we shall be able to examine the evolution of the ice growth, the ice distribution and the climatic variables during the glacial inception and also the subsequent glacial period.

Before carrying out this long run (results shown in section 4.4), we first wish to test the new version of the model and see whether in fact it is able to simulate the last glacial inception at around 119 kyr BP. By running different sensitivity experiments for the period 122 to 110 kyr BP, we wish to test the sensitivity of the MPM to changes of some parameters. We also wish to obtain the best configuration (parameter values) for the MPM, i.e., the one that simulates realistic present-day and interglacial warm climates and also produces ice growth (after the glacial inception) that is most consistent with the paleoclimatic data. These sensitivity experiments are described further below in sections 4.3.1 to 4.3.5. The new results will then be compared with those of Wang and Mysak (2002), in order to determine the effects resulting from the modifications added to the MPM. We shall see below that the addition of grasses and forests has generally decreased the surface albedo in the MPM, modifying the energy budget at the land surface. The incorporation of a new SED taking clouds into account has also changed the energy exchanges in the atmosphere and at the land surface. The addition of vegetation and a new SED has therefore modified the energy budgets, and thus we want to determine the consequences of these changes on the simulation of the last glacial inception.

#### 4.3 First run and parameter tuning

The model was run between 122 kyr BP and 110 kyr BP, using the same forcing fields that were used in Wang and Mysak (2002), i.e., the Milankovitch forcing (Berger, 1978) and Vostok-derived atmospheric  $CO_2$  levels (Barnola et al., 1999). The results of this first run were disappointing: they showed a strong and rapid ice growth over Tibet in Eurasia and almost no ice formation over North America. The first problem was due to changes in albedo in the lower Eurasian latitudes, i.e., over the Tibetan plateau, that induced an unrealistic ice growth. This is discussed in section 4.3.1. The second problem (very small ice growth over North American high latitudes) was due to the fact that with vegetation and a new SED the global climate for both glacial and interglacial periods was much warmer than the one simulated in Wang and Mysak (2002). Many sensitivity experiments were done that involved modifying parameters linked to clouds (sections 4.3.2 and 4.3.3), vegetation (section 4.3.4) and freezing of rain/refreezing of meltwater (section 4.3.5), in order to find the best parameter configuration for this new version of the MPM.

#### 4.3.1 Tibet plateau

The Tibetan plateau is the highest plateau in the world, with an average altitude of 4500 m. The elevation cooling effect of orography is parameterized in the model by decreasing the SAT linearly with height using a lapse rate of 6.5°C/km (Wang and Mysak, 2002). Temperatures over the Tibetan plateau are thus low due to the very high altitudes. Moreover, the addition of a new land surface component increases the albedo in this desert area, which cools down the climate further. Finally, ice is already present in small quantities at some places, and the ice-albedo feedback contributes also to the cooling, leading to a huge and early increase of ice volume over the Tibetan plateau, that may not be realistic.

The buildup of this large ice sheet over Tibet indicates a potential problem of the model. The complicated ice growth and decay processes cannot be resolved in the MPM. In order to eliminate this problem over Tibet, we prescribe an ice sheet thickness of 2 m and prevent it from growing further, even if the climate cools down significantly. This is quite realistic for our study period, since the ice developed at high northern latitudes after the last glacial inception and never reached these southern latitudes (30 to 45°N). The MPM now simulates a reasonable and later buildup of the Eurasian ice sheets, in the higher northern latitudes. The volume of ice over Eurasia will hereafter be representative of the ice sheets forming in high northern latitudes. Since the ice sheet height over the Tibetan plateau is fixed at a small value, this sheet makes a negligible contribution to the total Eurasian ice volume.

#### 4.3.2 Outgoing longwave radiation and cloud amount

The cloud amount distribution is prescribed in our model, as noted in section 3.2. It represents the total amount of clouds in a vertical column of air. The outgoing longwave radiation (OLR) is parameterized as being a value for clear sky minus a value representing the influence of clouds. The clear sky value depends on the surface air temperature. The cloudy sky part is the cloud amount multiplied by a positive factor  $k_{OLR}$ . Therefore, the larger the cloud amount, the smaller is the OLR. For a larger cloud amount, more energy is trapped between the surface and the atmosphere (cloud layer) and less OLR escapes to space. The prescribed cloud amount data used in the MPM contain some uncertainties. Since the proportionality factor  $k_{OLR}$  was initially chosen quite arbitrarily, we can slightly modify this parameter and find the best one.

In order to cool down the climate, we increase the OLR between 30 and 75°N, i.e., at latitudes where ice sheets are built up. We carried out different sensitivity experiments by progressively increasing the OLR. From Figure 4.1, we see that the

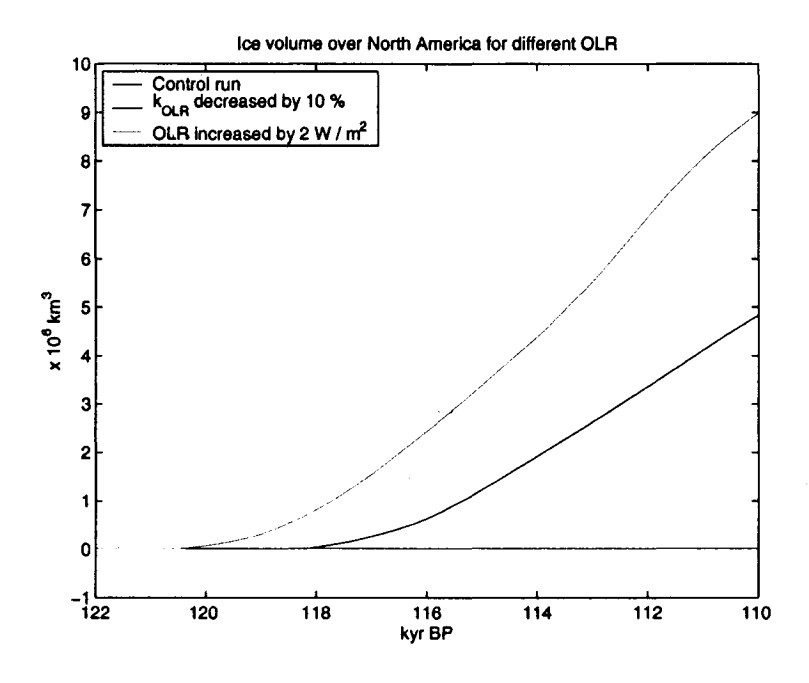


Figure 4.1: Ice volume growth over North America, simulated by the MPM, with an outgoing longwave radiation (OLR) similar to Z.Wang et al. (2004) (blue), an increased ORL corresponding to a 10 % decrease of  $k_{OLR}$  (red), and an ORL increased by a constant value of 2 W/ $m^2$  (green).

increase of the OLR led to a larger simulated ice buildup over North America, up to  $4.8 \times 10^6 \ km^3$  of ice by 110 kyr BP when the OLR is increased due to a 10% reduction of  $k_{OLR}$ . The only way to obtain ice over Eurasia was to substantially increase the OLR by a constant value, and thus to suppress the proportionality with the cloud amount. By increasing the OLR by  $2 \ W/m^2$ , we cooled down the climate substantially and formed up to  $9.0 \times 10^6 \ km^3$  of ice over North America and  $1.9 \times 10^6 \ km^3$  over Eurasia. Even if the results seem the best for the third scenario, it is not realistic to assume that clouds have no effect on the OLR. More plausible results for ice growth are therefore obtained by decreasing  $k_{OLR}$  by 10% (the second scenario). It produces good results for North America, where we observe consistent ice volume growth in this colder climate, even if the values reached at 110 kyr BP are still too low, compared to paleoclimatic data. The 10% increase of  $k_{OLR}$  will thus be used in future runs.

#### 4.3.3 Cloud optical depth

The cloud optical depth is prescribed at each grid of the MPM (see section 3.2) and has an uncertainty of 30% (Pincus et al., 1995; Zhang et al., 1995). The planetary albedo is also underestimated in the MPM, i.e., it is lower than the satellite data (ERBE) (Z.Wang et al., 2004). This underestimation contributes to the warm bias in the MPM. Since the modelled climate with dynamic vegetation is still slightly too warm, it is reasonable to increase the cloud optical depth uniformly to cool down the climate. A larger optical depth induces a larger reflection of the incident solar rays, as well as a smaller transmission through the atmosphere.

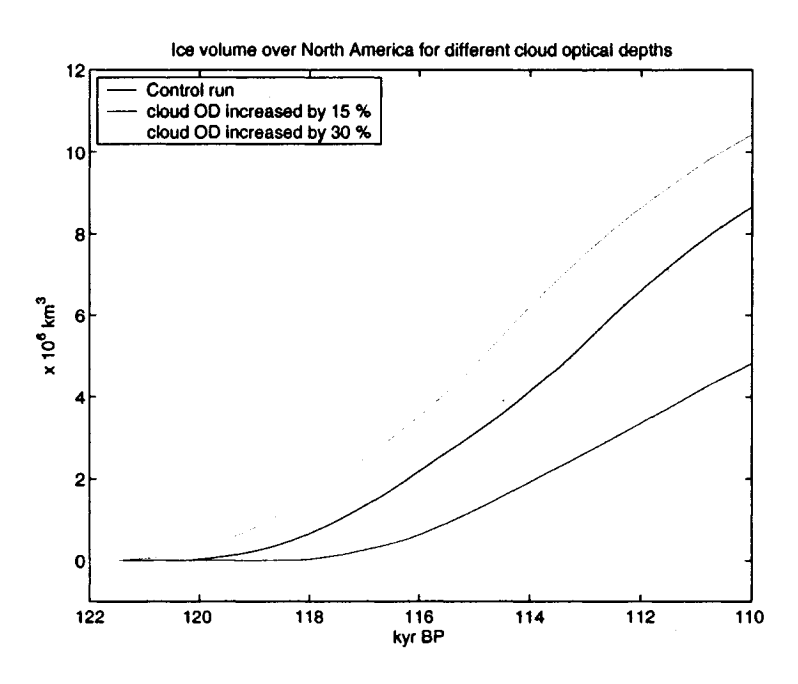


Figure 4.2: Ice volume growth over North America, simulated by the MPM, with the cloud optical depth (OD) as in Z.Wang *et al.* (2004) (blue), a cloud OD increased by 15 % (red), and a cloud OD increased by 30% (green).

For an increase of 15%, we observe for the first time a growth of the Eurasian ice sheet, up to  $1.6 \times 10^6 \ km^3$  by 110 kyr BP (not shown here), and a better growth of the North American ice sheet, up to  $8.6 \times 10^6 \ km^3$  in 110 kyr BP (Figure 4.2). For a larger increase than 15%, ice appears over central North America for the present-day

simulation, which is not realistic. The 15% increase will thus be used in future runs.

#### 4.3.4 Vegetation albedos

The greening of the MPM, by the addition of a dynamic vegetation component and an improved land surface scheme, leads to a decreased land albedo in most regions and a warmer climate over areas covered by trees or grasses. Different sensitivity experiments were run in order to determine the effect of the response of the climate to vegetation albedos that are larger than the ones used in the BATS model (see section 3.3).

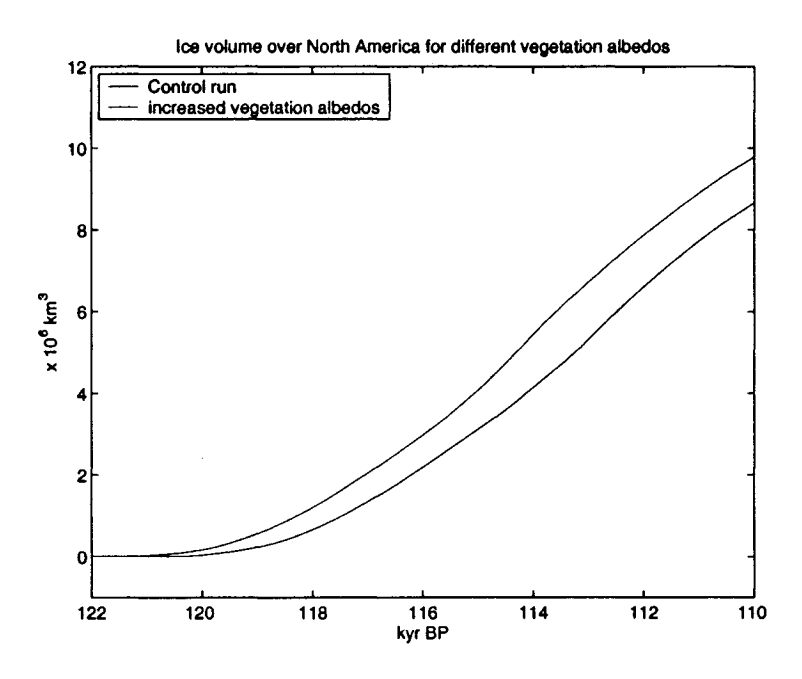


Figure 4.3: Ice volume growth over North America, simulated by the MPM, with tree/grass/desert albedos similar to the BATS model (red) and with increased albedos for trees and grasses (blue) (see text below for albedo values)

Increasing slightly the albedos of trees and grasses from the values used in BATS, namely 0.12/0.16 respectively, to 0.18/0.20 cools down the climate. The albedo of desert is fixed at 0.35. Consequently, the model simulates 13 % more ice over North America at 110 kyr BP, as seen in Figure 4.3. We can therefore assume that the ad-

dition of vegetation in the MPM, and the consequent decrease of albedo, contributed to the warming of the climate.

Even if the increase of ice volume is greater with higher albedos, it is not realistic to use these high values since the values chosen in the BATS model are already the maximum ones that are allowed for consistency with the other parameterizations of the land surface model. We thus decide to keep the albedo values from BATS, i.e., 0.12/0.16/0.35 for the tree/grass/desert albedos.

#### 4.3.5 Freezing of rain / Refreezing of meltwater

As described in Wang and Mysak (2002), the parameterization of the freezing of rain and refreezing of meltwater is quite simple. When the permanent snow-depth (defined as snow-equivalent depth of ice in August) exceeds 2 m in one grid cell, 60% of liquid water composed of rainfall and melted snow is converted into ice. This value of 60% comes from Greenland ice sheet studies, and it is used for other ice sheet investigations in glacial periods (see Wang and Mysak (2002) for more details). However, values other than 60% have been proposed by others and it has also been suggested that this value cannot be valid uniformly for all regions (Janssens and Huybrechts, 2000). The use of the constant 60% value therefore adds a limitation to the model.

One sensitivity experiment was first run by decreasing the permanent snow depth from 2 m to 1 m, but at the same time keeping a constant conversion percentage of 60%. Other sensitivity experiments were run by increasing the percentage of water converted into ice to 70 and 80%, with a constant permanent snow depth of 2 m for both cases. The last sensitivity experiment was run by simultaneously decreasing the permanent snow depth to 1 m and increasing the conversion percentage to 70%. The ice volume growth curves for these experiments are shown in Figure 4.4.

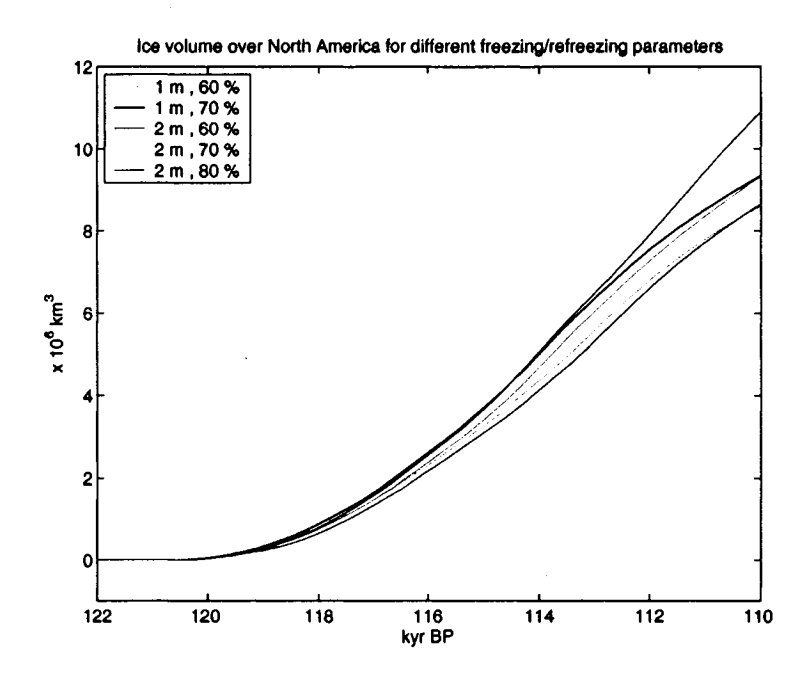


Figure 4.4: Ice volume growth over North America, simulated by the MPM, with different permanent snow depths and fractions of liquid water converted into ice: 1 m and 60 % (light blue), 1 m and 70 % (black), 2 m and 60 % (red), 2 m and 70 % (green), and 2 m and 80 % (magenta).

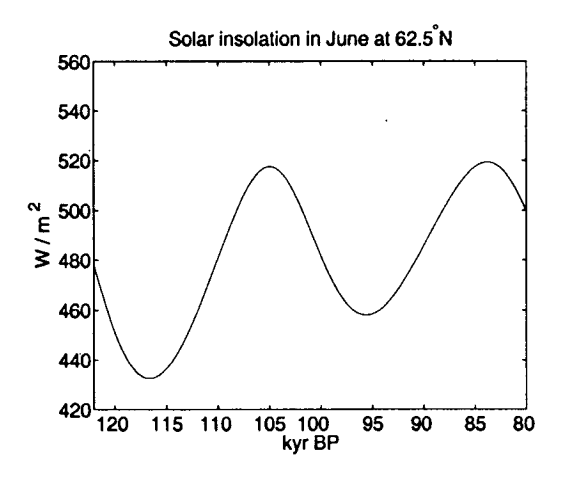
If we decrease only the critical snow depth to 1 m and keep the fraction of liquid water converted into ice constant at 60%, there is almost no increase of the ice volume. This agrees with the observations of Wang and Mysak (2002), saying that the ice sheet growth was not very sensitive to changes in the critical snow depth. By modifying only the fraction of liquid water converted into ice, from 60 to 70%, the North American ice volume at the end of the run is increased by 8%. If the fraction of liquid water converted into ice is increased to 70% and the critical snow depth is decreased to 1 m, we obtain the same ice volume increase (8%). Finally if the conversion percentage is increased from 60% to 80%, the North American ice volume at the end of the run is increased by 26%.

Our results demonstrate that a change of the fraction of liquid water converted into ice produces a sensible change in ice sheet growth. However, the results obtained with the parameters used by Wang and Mysak (2002), i.e., a permanent snow depth of 2 m and 60% of water converted into ice, already show a consistent ice sheet growth over

northern latitudes. In order to compare our results with the ones obtained by Wang and Mysak (2002), we will therefore continue our experiments with these parameters.

#### 4.4 Results of the long run

The model was then run between 122 kyr BP and 80 kyr BP, using observed forcing fields that are the temporal extension of those used in Wang and Mysak (2002). These are the Milankovitch forcing (Berger, 1978) and Vostok-derived atmospheric  $CO_2$  levels (Barnola *et al.*, 1999) shown in Figure 4.5.



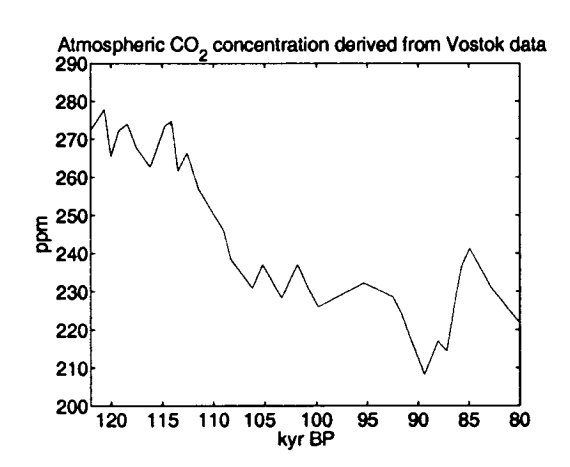


Figure 4.5: Solar insolation at a high northern latitude in summer (left) due to Berger (1978) and Vostok-derived  $CO_2$  concentration (right) due to (Barnola et al., 1999), between 122 and 80 kyr BP.

#### 4.4.1 Ice volume

Figure 4.6 illustrates the evolution of North American, Eurasian and total ice volumes simulated by the "green" MPM between 122 and 110 kyr BP. The Greenland ice sheet is not included in any of the above volumes. Compared to the results of Wang and Mysak (2002) obtained with the earlier version of the MPM, we obtain a larger North American ice volume, a smaller Eurasian one, and together, a slightly smaller total

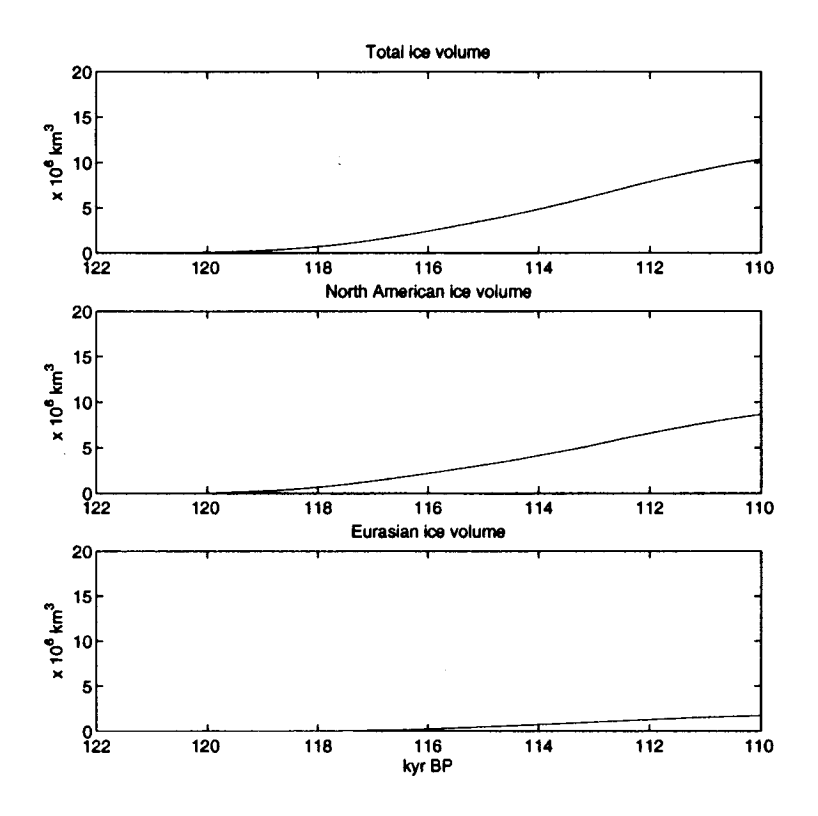


Figure 4.6: Total ice volume simulated by the MPM between 122 and 80 kyr BP (top); ice volume over North America (middle) and over Eurasia (bottom) for the same run.

ice volume ( $10.3 \times 10^6 \ km^3$  versus  $13 \times 10^6 \ km^3$  in Wang and Mysak (2002)). The addition of forests over Europe warmed up the area enough to prevent significant ice buildup there, in contrast to the case found in Wang and Mysak (2002).

Figure 4.7 shows the ice volume over North America and Eurasia simulated between 122 kyr BP and 80 kyr BP, as well as the total ice volume, which includes Greenland (not included in Figure 4.6). The ice volume is much lower over Eurasia than over North America, in agreement with the reconstructions of Peltier (1994). The North American ice volume increases rapidly from 119 to 110 kyr BP and then slowly increases, reaching 13.6 x  $10^6 \ km^3$  at 80 kyr BP. The Eurasian ice volume increases slowly until 95 kyr BP, after which time it increases more rapidly, reaching a final volume of 5.2 x  $10^6 \ km^3$  at 80 kyr BP. The Greenland ice volume actually decreases slightly (about 7 %) between 122 and 80 kyr BP. However, this change

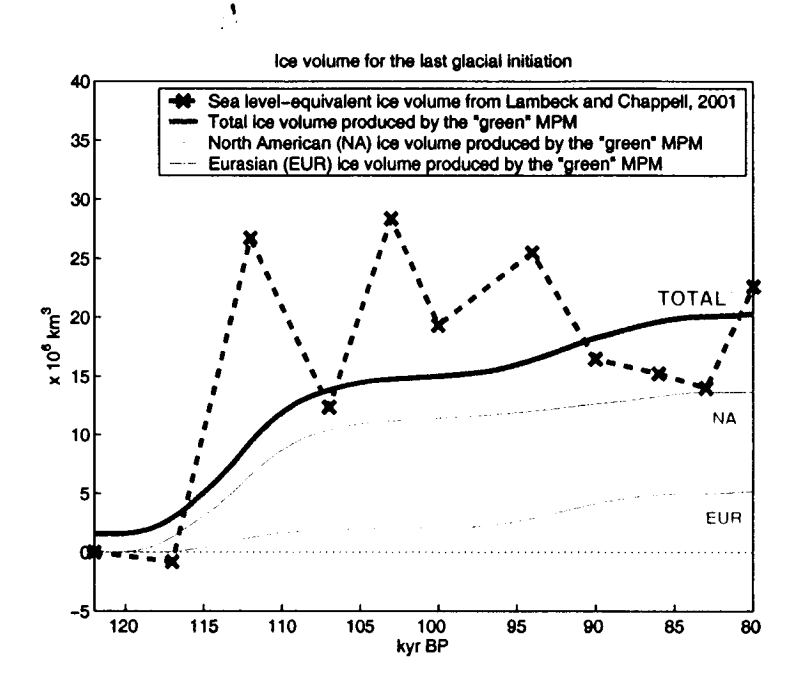


Figure 4.7: Total ice volume (bold green) simulated by the MPM between 122 kyr BP and 80 kyr BP, ice volume over North America (NA) and Eurasia (EU), and the sea-level equivalent ice volume from Lambeck and Chappell (2001).

is negligible compared to the total ice volume change. The general cooling of the climate induces reduced temperatures and precipitation over Greenland, and hence a reduction of the snow accumulation rate. As a consequence, there is a drop of the surface elevation of the Greenland ice sheet. The total ice volume simulated over the Northern Hemisphere by 80 kyr BP is  $19.9 \times 10^6 \ km^3$ .

The red crosses in Figure 4.7 show the sea level-equivalent ice volume determined by Lambeck and Chappell (2001) at different times. During the Quaternary, sea level changes were mainly due to the growth and decay of ice sheets. The changes in ice mass during glacial cycles and the time of glaciations are thus easy to deduce from sea level change data (Lambeck and Chappell, 2001). Information on the distribution of ice among the major ice sheets is more limited. Lambeck and Chappell (2001) plotted the sea level-equivalent icevolume changes from 140 to 20 kyr BP, estimated from observations of local sea level change at the Huon Peninsula, Papua New Guinea. Compared to these paleoclimatic data, our results show a total modelled ice volume

that is too smooth and too low for the period up to 95 kyr BP. After 95 kyr BP, our simulated total ice volume is comparable to the observations. However, our simulations only simulate the ice volume growth in the Northern Hemisphere up to 75 °N. Hence, we do not have any simulation of ice volume change north of 75 °N and in the Southern Hemisphere (Antarctica).

As explained in Lambeck et al. (2002), it seems that insolation controls the ice sheet buildup during the early part of the glacial cycle. But starting at about MIS-4 (around 75 kyr BP), feedback mechanisms and other processes become more important (e.g., iceberg calving from unstable ice sheets, shifts in ocean circulation) and the structure of the ice volume evolution shows high frequency fluctuations. The coarse resolution of the model prevents us from simulating these high frequency oscillations. That is why we did not continue the runs after 80 kyr BP, since the absence of thermodynamics in the ice sheet model as well as other internal climate feedbacks might have led to unrealistic simulations.

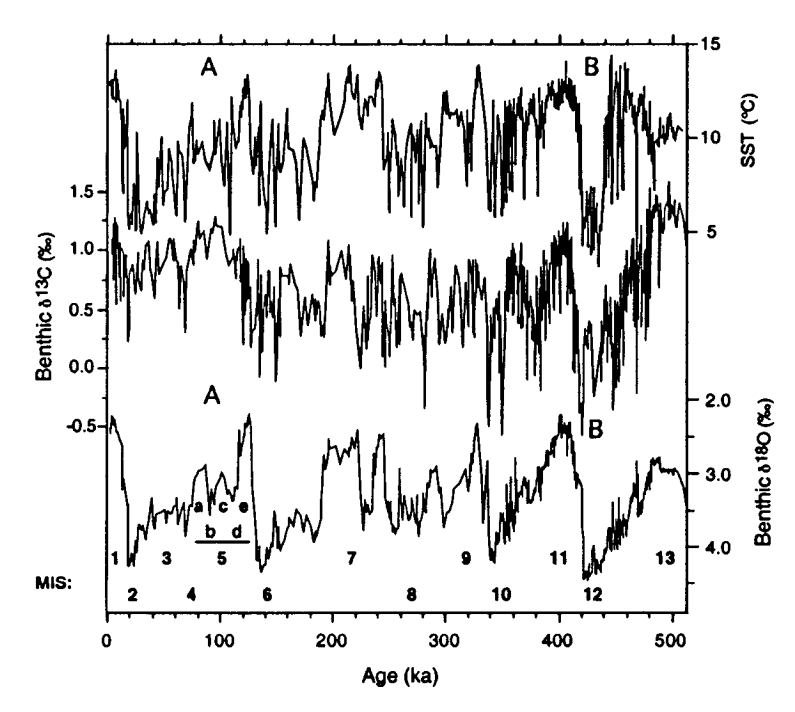


Figure 4.8: Paleoclimate data from ODP Site 980 ( 55°29′N, 14°42′W, 2179 m) over the last 0.5 million years (Wang et al., 2002).

Figure 4.8 shows paleoclimate data from Ocean Drilling Program (ODP) Site 980 in the northern North Atlantic (Oppo et al., 1998; McManus et al., 1999; Wang et al., 2002). From the top to the bottom, it displays the evolution for the last 500 kyr of the SST (as derived from  $\delta^{18}O$  measurements of planktic foraminifera, adjusted for ice volume using the benthic  $\delta^{18}O$ ), benthic  $\delta^{13}C$  (proxy for the strength of the THC in the North Atlantic) and benthic  $\delta^{18}O$  (proxy for global ice volume). Of interest here is the bottom curve, i.e., the evolution of benthic  $\delta^{18}O$ , which clearly delineates the glacial (even) and interglacial (odd) marine isotope stages (MIS). Our period of interest is the MIS-5, with the glacial inception as the transition MIS-5e/5d. The results obtained with the MPM do not display the interstadial stage MIS-5c; rather the simulation shows a monotonic increase of ice volume. The interruption in ice growth at MIS-5c might be due to an ice melting caused by increased summer insolation and a large discharge of ice sheets into the ocean. The fact that the modelled total ice sheet volume is lower than the observed, and the fact that the ice sheet model has no thermodynamics might be responsible for the absence of a large ice discharge.

#### 4.4.2 Ice distribution

Figure 4.9 (see page 56) shows the modelled distribution of ice sheets at 122, 116, 110, 100, 90 and 80 kyr BP. We note permanent ice first appearing at 116 kyr BP in the vicinity of the northern Laurentide, Cordilleran, Scandinavian and Siberian regions, and over Alaska. Between 116 kyr BP and 80 kyr BP, the ice sheets continue to expand longitudinally, towards the centre of the continents, as well as southward. At the end of the run, ice sheets are located over Alaska, northwestern Canada, northeastern Canada, northwestern Europe and eastern Russia. The ice sheets therefore progressively expand and thicken, as seen in Wang and Mysak (2002). However, our results show ice sheets over Eurasia that are considerably smaller than those simu-

lated in Wang and Mysak (2002), especially in the Scandinavian region, and the ice sheet over Alaska becomes much larger and thicker. Our results do not show any ice sheet buildup in the centre of North America, whereas there is permanent ice appearing on the western and eastern sides of the continent. At the end of the run, ice begins to reach this central area, but only due to the lateral expansion of the two ice sheets that surround it. In section 4.5, we shall discuss the possible reasons why ice is absent in the centre of North America during the majority of the runs.

Information about the growth and decay of the ice sheets before the LGM is practically non-existent, because any glacial records would have been mostly destroyed by the advance and retreat of the ice sheets during the last glacial cycle and because the materials that may have survived are too old for reliable radiocarbon dating (Lambeck and Chappell, 2001). We know, however, that regions of northern Canada, especially Baffin Island and the Queen Elizabeth Islands, are often considered as the places where the Laurentide ice sheet started to develop (Andrews et al., 1985, 1986; Clark et al., 1993). Results of our model display quite well the initial formation of the Laurentide ice sheet in this region. On the other hand, our results show the formation of a huge ice sheet over Alaska at the beginning of the glacial period. This might be due to the very cold temperatures simulated by the model in this area, which thus led to a rapid buildup of an ice sheet. The model indeed displays a cool bias in winter in the southern part of Alaska (as explained in section 4.5). Geologic records do not show any ice sheet over Alaska at the time of the LGM, but there is no real evidence of ice at the time of the glacial inception. It is therefore an open question as to whether an Alaskan ice sheet built up at the glacial inception and then disappeared, or whether Alaska has always been ice-free.

Lambeck et al. (2002) suggested that some ice sheets may form and then disappear during glacial periods. They explained that, during the late stages of the last interglacial, warm conditions prevented the Arctic sea-ice cover from extending too far south. The moisture supply to polar regions was therefore enhanced and led to

snow accumulation. When temperatures decreased, ice sheets built up, and the sea ice area increased. The subsequent cooling led to a precipitation shadow north of the Laurentide ice sheet, causing the northern ice to decay at the same time as the maximum southern limit was reached. This discontinuity in the formation of ice sheets has been observed over western Canada and over Eurasia. Records of the development of the Laurentide ice sheet thus indicate a very dynamic ice sheet, with rapid ice-sheet growth as well as decay during the last glaciation (Andrews and Tedesco, 1992; Bond et al., 1992; Clark et al., 1993). Svendsen et al. (1999) showed also that the major Eurasian glaciation began over Arctic Russia (Kara Sea), but the ice sheets later moved from this area, and it was finally free of ice by the very cold LGM (MIS-2). Finally, the Scandinavian ice sheet also experienced successive growth and decay periods between MIS-5d and MIS-4 (Helmens et al., 2000; Mangerud, 2004 in press).

Some model studies showed that there was no buildup of an ice sheet over Alaska at the glacial inception. Vettoretti and Peltier (2003b) suggested that their GCM did not simulate perennial ice cover over Alaska and Scandinavia at 116 kyr BP because an increased northward heat and moisture transport by transient eddies maintained sufficient snowmelt in summer over these two regions. The Canadia Arctic Archipelago and eastern Siberia were, on the other hand, regions where the northward latent and sensible heat transports by transient eddies were reduced, and where we observed ice nucleation (Vettoretti and Peltier, 2003b). The zonal spatial heterogeneity of ice nucleation zones was therefore in part a result of increases and decreases in northward transport of latent and sensible heat. In the MPM, the transient eddies are parameterized as a diffusion process. Due to the coarse resolution of the model, there is no spatial heterogeneity for heat and moisture transport over North America. The model is not capable of simulating changes in moisture transport pathways as ice sheet growth alters continental topography. This might be one reason to explain the buildup of a huge Alaskan ice sheet in our simulations.

### 4.4.3 Evolution of the climate and the THC between 122 and 80 kyr BP

Figure 4.10 (see page 57) shows the evolution of the global annual mean SAT, the maximum THC intensity, the January SAT over northern North America and over the northern North Atlantic, as simulated by the MPM between 122 and 80 kyr BP. We choose to display the January SST in order to study the relation between the maximum cooling of the water and the evolution of the THC. We also display the January SAT over North American high latitudes in order to compare the cooling over land and over the ocean.

From Figure 4.10a, we note an overall global SAT decrease of  $2.7^{\circ}C$  by 80 kyr BP. The SAT in January at 72.5°N over North America and the North Atlantic display a similar evolution with decreases of 5.1°C over North America and 5.7°C over the North Atlantic (Figure 4.10c and d). The maximum intensity of the THC, on the other hand, shows an overall increase of 7.4 Sv by 80 kyr BP (Figure 4.10b). Wang and Mysak (2000) showed that the THC increased during the initiation of a glacial period, due to the decreased freshwater input and the cooler SST at high latitudes that increased the density of the water at the sinking region. In our results, we also observe this strong cooling of SST at latitudes where deep water forms (Figure 4.10d) and we also see a decrease of precipitation at these latitudes (not shown here). Wang and Mysak (2000) explained that this stronger THC led to an increased land-sea thermal contrast at high latitudes and hence to a bigger moisture transport from the ocean to the land, which forms part of an optimal configuration for delivering moisture to the Laurentide Ice Sheet. Moreover, Johnson and Andrews (1979) and Peltier (1994) showed that about 50% of the maximum ice volume during the last glaciation had accumulated within the first 10 kyr of the 100 kyr glacial period, due to an abundant moisture supply from subpolar oceans and from lower latitudes. By comparing the January SAT over North America and over the North Atlantic modelled by the MPM

between 122 and 95 kyr BP, we also observe an increase of the contrast between the SAT over land and over the ocean.

The temperature and THC time series in Figure 4.10 all show a similar irregularity around 89 kyr BP: this is probably due to the drop in the orbital forcing prior to 95 kyr BP, as shown on Figure 4.5 (left panel). This decrease of the summer solar insolation reduces the melting of ice at high latitudes and induces, with a small time lag, a stronger growth of ice sheets over northern Europe, as seen in Figure 4.7 and 4.9. The extension of the ice sheets area increases the surface albedo and reduces the solar absorption by the ground; it contributes thus to the cooling of the surface air temperature (Figure 4.10c and d). The increase of ice volume furthermore reduces the freshwater input into the ocean and leads consequently to an increase of the THC at around 90 kyr BP, as seen on Figure 4.10b. The THC thus responds quite rapidly to the freshwater input changes. This anomaly disappears after several kyr.

### 4.4.4 A critique of the downscaled atmospheric data used in the MPM

In order to downscale the sectorially averaged SAT, precipitation and surface specific humidity to a 5° x 5° grid over North America and Eurasia, Wang and Mysak (2002) used present-day output of the UK Universities Global Atmospheric Modelling Program (UGAMP) AGCM and calculated the deviations from the sectorially averaged values. These anomalies simulated by the AGCM were then used to build a 2-D grid of atmospheric variables over northern latitudes  $(30 - 75^{\circ}N)$ . Since these anomalies were determined from UGAMP model results, we want to check here if they are really consistent with observational data and that they do not introduce some systematic biases that could lower the accuracy of our results.

We compared present-day observations from the ECMWF with the AGCM results

that we used for downscaling. We concentrated our study on comparing the longitudinal deviations from the sectorially averaged SAT in January and July. We found a warm bias in the AGCM data over the centre of Canada, with SAT anomalies given by the AGCM being up to 6.5°C higher in winter and 7.1°C higher in summer in the latitude band 70-75 °N than those given by ECMWF. We also detected a strong warm bias in southwestern North America, but this region is too far from the area of ice formation, and this warm bias will not influence the glacial inception. Finally, we observed a cold bias in the AGCM data over southern Alaska, with the SAT deviations being up to 11.5°C lower than the ECMWF deviations in January. The warm bias in central Canada may have led to the summer melting of the ice built up in this area in the MPM. Hence we simulated no permanent ice between 60 and 80° of longitude, in the first 20 kyr of the run. Finally, the cold bias over Alaska in winter may explain why the MPM simulates such a large and deep ice sheet over this area.

By running the model with the SAT anomalies from the ECMWF, but using AGCM data for the precipitation and surface specific humidity, we found that the MPM simulates the slow buildup of an ice sheet in central North America. The simulated ice sheet extent over Eurasia, however, was also considerably greater, especially in the western side of Eurasia. Thus using ECMWF anomalies for SAT partially fixes the problem over central North America, but leads to an Eurasian ice sheet that is too large compared to paleoclimatic data. Such a run is, however, of limited value because we only changed the SAT anomalies, and not the precipitation and surface specific humidity anomalies.

In both cases (AGCM and ECMWF data), we know, however, that there are two important limitations in using these SAT, precipitation and surface specific humidity anomalies in our last glacial inception run. The first limitation is due to the fact that we use present-day anomalies, assuming that the present climate is very similar to the climate at 122 kyr BP. The second limitation is due to the fact that these anomalies remain constant during the whole run. This is not realistic since

the progressive buildup of ice sheets over North America and Eurasia will obviously change the climate over these areas, especially the atmospheric circulation. The SAT anomalies might therefore be different. The anomalies from the ECMWF or from the AGCM are thus both introducing strong limitations in the simulation of the last glacial inception.

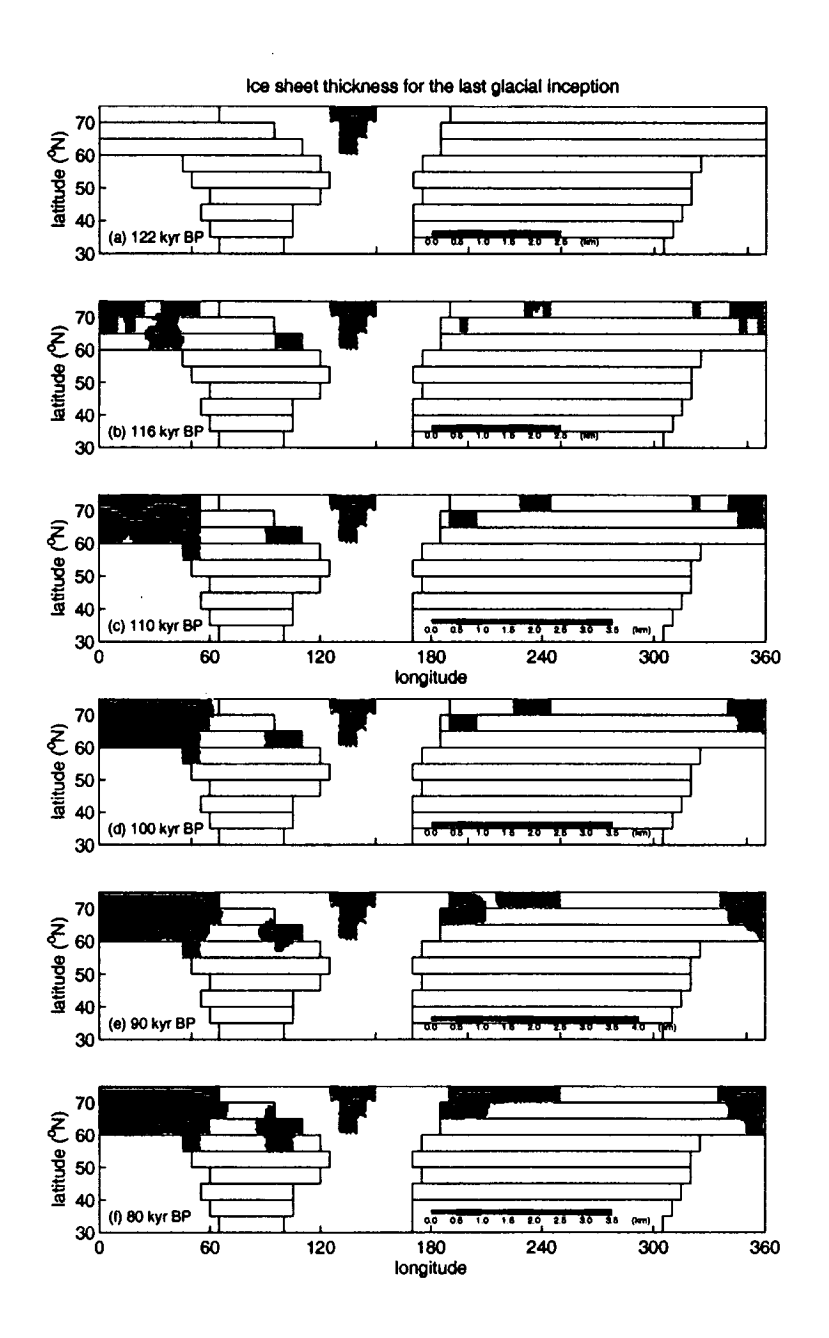


Figure 4.9: Ice sheet distribution simulated by the MPM between 30 and 75° N at 122 kyr BP (a), 116 kyr BP (b), 110 kyr BP (b), 100 kyr BP (d), 90 kyr BP (e), and 80 kyr BP (f).

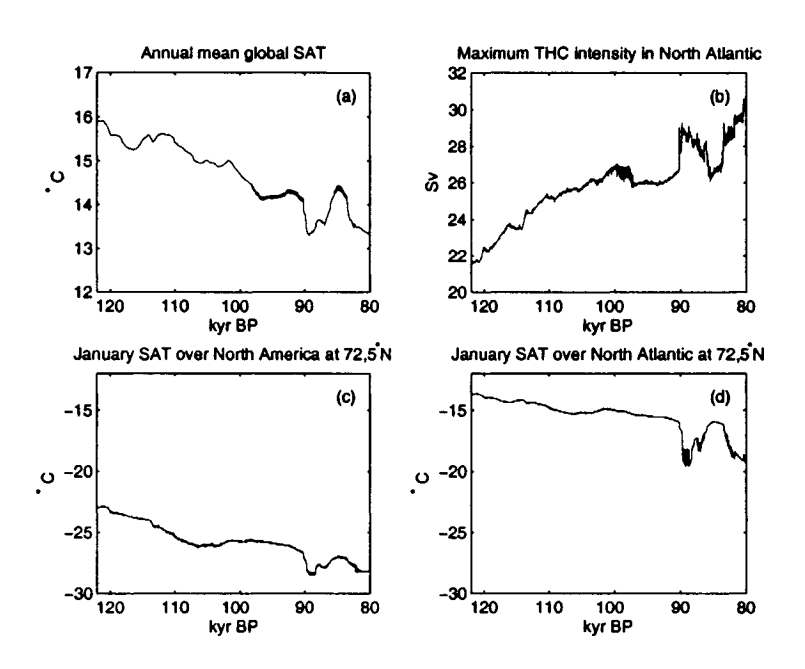


Figure 4.10: Evolution of climatic variables simulated by the MPM between 122 and 80 kyr BP: (a) Annual mean global SAT, (b) maximum THC intensity in the North Atlantic, (c) SAT in January over North America at  $72.5^{\circ}N$ , and (d) SAT in January over the North Atlantic at  $72.5^{\circ}N$ .

#### Chapter 5

# Simulation of future climate changes

## 5.1 Earlier studies about long-term future climate changes

Kukla et al. (1972) suggested that the present interglacial has already lasted too long and would end very soon. Hence they predicted an imminent abrupt glaciation. Broecker (1998) also suggested that the present interglacial should end abruptly, as was the case for the past interglacials. But he was uncertain about the date of the next glacial inception and how the natural evolution of the climate might be modified by the anthropogenic increase of greenhouses gases in the atmosphere and changes in deep water formation.

A number of groups have carried out the simulation of future climate changes on a geologic time scale. General Circulation Models could not be used for these long-term simulations because of their long computational time. Berger et al. (1991)

made a review of models of different complexity which were used between 1970 and 1990 to simulate future long-term climate changes. These models did not take into account the variations of the atmospheric  $CO_2$  concentration, and ran simulations with a constant  $CO_2$  concentration of  $\sim 225$  ppm, as an average of the  $CO_2$  levels during the glacial-interglacial cycles. These different models predicted a slow cooling trend which started at 6 kyr BP and continued for the next 5 kyr. This was then followed by a cold interval at around 25 kyr AP and a major glaciation at around 55 kyr AP. However, after a detailed study of the links between summer solstice solar radiation and ice volume, Ledley (1995) suggested that the present interglacial may last until 70 kyr AP.

Other studies were performed using a number of other atmospheric  $CO_2$  concentrations. Saltzmann et al. (1993) showed that a CO<sub>2</sub> concentration maintained at 350 ppm over a long period of time could place the climate in a stable non-oscillating regime characterized by a lower ice mass and a possible retreat of the Greenland and Antarctic ice sheets. This could mark the end of the Quaternary period and the beginning of an almost ice-free climate regime. Loutre and Berger (2000a) ran the LLN model with constant  $CO_2$  concentrations ranging from 210 to 290 ppm and with present-day conditions for the ice sheets as initial conditions. For a concentration of 210 ppm, a glaciation started very quickly and the Next Glacial Maximum peaked at 101 kyr AP. For a concentration lying between 220 and 280 ppm, the quite stable present interglacial lasted at least until 55 kyr AP, i.e., considerably longer than the preceding interglacials. The ice volume then started to grow considerably, the amplitude of this growth being  $CO_2$ -dependent. Finally, for a  $CO_2$  concentration of 290 ppm, the LLN model did not simulate any glacial inception for the next 130 kyr. Moreover, for a concentration higher than 250 ppm, the LLN model simulated a melting of the Greenland ice sheet during the first 50 kyr; however, this ice sheet grew back after the glacial inception.

In contrast to the above studies, there have been several model investigations

in which a variable atmospheric  $CO_2$  scenario has been used as an external forcing. Oerlemans and Van der Veen (1984) used a simple ice sheet model and forced it with a  $CO_2$  concentration similar to that of the last two major terminations. They predicted a long interglacial lasting another 50 kyr, followed by a first glacial maximum at around 65 kyr AP, a slight melting at around 80 kyr AP and the next glacial maximum at around 110 kyr AP. Using a model of intermediate complexity (the LLN model), Loutre and Berger (2000a) ran long-term simulations with a "natural"  $CO_2$  scenario: the evolution of the  $CO_2$  concentration for the next 130 kyr was the same as the one for the past 130 kyr, as reconstructed from Vostok ice core data (Jouzel et al., 1993; Petit et al., 1999). They simulated a long present interglacial lasting about 50 kyr. Loutre and Berger (2000a) then used a  $CO_2$  scenario labelled "Global Warming": the  $CO_2$  concentration linearly increased during the next 200 years, from 296 ppm to 750 ppm, and then slowly decreased during the following 800 years to a value of around 280 ppm. Then the  $CO_2$  followed during the next 130 kyr the "natural"  $CO_2$  scenario from Vostok. Their results showed that Greenland almost completely melted between roughly 10 and 14 kyr AP, and then reformed slowly between 15 and 50 kyr AP. After 50 kyr AP, ice sheets started to grow elsewhere, but the ice volume was lower than the one obtained without the global warming episode. After 70 kyr AP, the evolution of the total ice volume approached the one obtained with the "natural  $CO_2$  scenario" and the climate system was no longer sensitive to what could happen to the  $CO_2$  over the next few centuries. Berger and Loutre (1996) had previously run a similar simulation to the above, but with a peak of 550 ppm (instead of 750 ppm) in the "Global Warming" scenario. In this case there was only a slight melting of Greenland during the first 1000 years. Their results suggest that there is a threshold value of atmospheric  $CO_2$  above which the Greenland ice sheet disappears in long-term simulations of the LLN model.

#### 5.2 Which scenario for $CO_2$ ?

As explained in section 2.3, the atmospheric  $CO_2$  concentration has continuously increased since the Industrial Revolution, from 280 ppm to 373 ppm today. Furthermore, it is likely to continue increasing for the next one or two centuries (Houghton et al., 2001). We are today in a period of anthropogenically-induced warming that has not been experienced before. The processes regulating the atmospheric  $CO_2$  concentration are quite complex and involve different physical, chemical and biological feedbacks. The total amount of  $CO_2$  emitted into the atmosphere by different sources (e.g., burning of fossil fuels, deforestation, etc.) is also uncertain. It is thus difficult to determine what will be the future evolution of the  $CO_2$  concentration.

Different scenarios have been proposed by the Intergovernmental Panel on Climate Change (Houghton et al., 2001) for the short-term future atmospheric  $CO_2$  concentration. The "business as usual" scenario (scenario IS92a) represents a 1 % increase per year compounded of the  $CO_2$  concentration. Forty other scenarios have been created to replace the IS92 scenarios, and these are given in the SRES (Special Report on Emission Scenarios). They take into account the growth or otherwise of the human population, the changes in industrial activity and the environmental restrictions imposed by governments on greenhouse gas emission. The range of scenarios in the SRES portrays that the atmospheric  $CO_2$  concentration may reach 540 to 970 ppm by 2100, i.e., 90 to 250 % above the pre-industrial concentration of 280 ppm in 1800. Allowing for uncertainties around each scenario, especially that concerning the magnitude of the feedback on radiative forcing from the terrestrial biosphere, the total range given in the SRES is from 490 to 1260 ppm.

Since the MPM does not include an active carbon cycle, we have to prescribe a  $CO_2$  scenario and use it as an external forcing. We first ran various short-term simulations with increasing atmospheric  $CO_2$  concentration, followed by a stabilization of the  $CO_2$ . The objective was to see if the MPM, despite being a model of intermediate

complexity, was able to respond sensibly to short-term modifications in the  $CO_2$  forcing. The results of these experiments are shown in sections 5.3.1 and 5.3.2. We then ran long-term simulations, for the next 100 kyr, in order to determine when the next glacial inception might occur. We first forced the MPM with constant  $CO_2$  concentrations ranging from 210 to 370 ppm (section 5.4.1). We finally ran the same simulations but with a global warming episode during the first 1.2 kyr of the run (section 5.4.2).

#### 5.3 Short-term runs

#### 5.3.1 The canonical 2 x $CO_2$ experiment

In Petoukhov et al. (2004b), the MPM and seven other models of intermediate complexity were run to simulate the response of the climate to the doubling of atmospheric  $CO_2$  concentration followed by a constant stabilization. Their results were both intercompared and compared with GCMs results for  $CO_2$  doubling. The scenario used for atmospheric  $CO_2$  concentration started at 280 ppm and then consisted of a monotonic increase of  $CO_2$  concentration at a rate of 1 % per year compounded for the first 70 years; this was followed by a stabilization at the 560 ppm level over a period longer than 1500 years. The version of the MPM used in the study of Petoukhov et al. (2004b) did not include the new solar energy disposition or the vegetation component described in section 3.2 and 3.3; furthermore, the ice sheet component was an isothermal 1-D model.

Using the realistic solar forcing calculated by Berger (1978), we ran the "green" MPM for 5000 years, starting with the pre-industrial value of  $CO_2$  at year 1800 (280 ppm) followed by the same scenario for the atmospheric  $CO_2$  concentration used in Petoukhov *et al.* (2004b) (Figure 5.1): this is the "equilibrium 2 x  $CO_2$ " run.

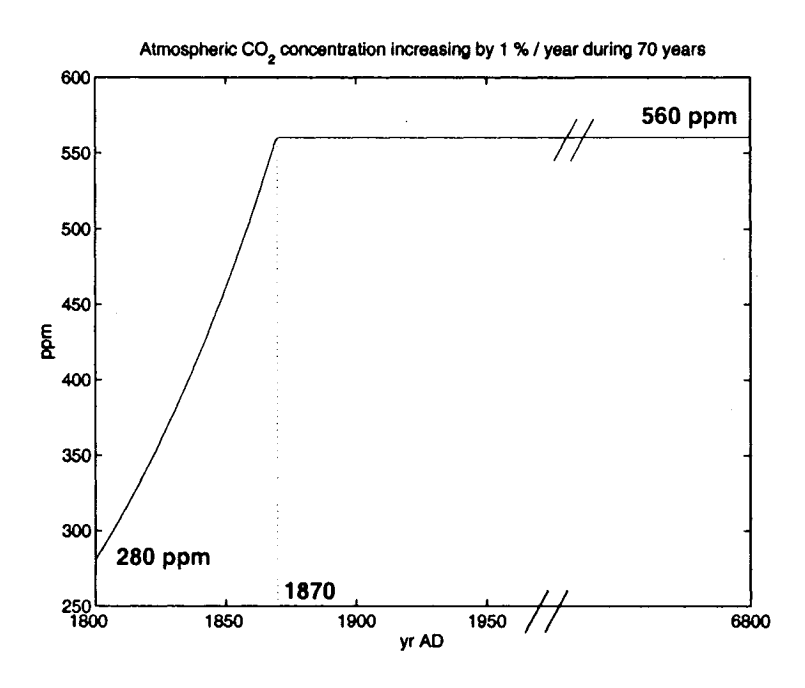


Figure 5.1: Atmospheric  $CO_2$  concentration for the "2 x  $CO_2$  experiment".

We compared first the climate at the end of the "equilibrium 2 x  $CO_2$ " run with the climate at the end of the "equilibrium 1 x  $CO_2$ " run (the model run for 5000 years with a constant  $CO_2$  concentration of 280 ppm). The surface air temperature and outgoing longwave radiation flux were both greater for the "equilibrium 2 x  $CO_2$ " run because of the  $CO_2$ -induced warming. The difference was even greater at high latitudes, and particularly at high southern latitudes during the Southern Hemisphere winter. We believe the latter is due to the melting of sea ice in the Southern Hemisphere and the strong ice-albedo feedback. There was a particularly noticeable decrease of the albedo in the polar southern latitudes during austral summer. Our results also show an increase of precipitation near the equator and in subpolar and polar regions, the latter being likely due to an increase of the meridional poleward moisture transport.

We next compared our results, for the first 1500 years, with those obtained by the old version of the MPM presented in Petoukhov et al. (2004b). The new MPM simulated a larger SAT increase in high northern latitudes, especially in summer (4.5°C, versus 2.9°C in Petoukhov et al. (2004b)). This might be due to the addition

of vegetation and the subsequent biogeophysical vegetation-albedo feedback. The presence of the vegetation in the model contributes to the decrease of the surface albedo and to the increase of atmospheric moisture. As a consequence, there is an increase in the energy absorbed by the climate system at higher northern latitudes in summer. Our results also showed that the precipitation changes simulated by the new version of the MPM were generally larger than those simulated by the old version (Petoukhov *et al.*, 2004b), due to the vegetation - temperature feedback.

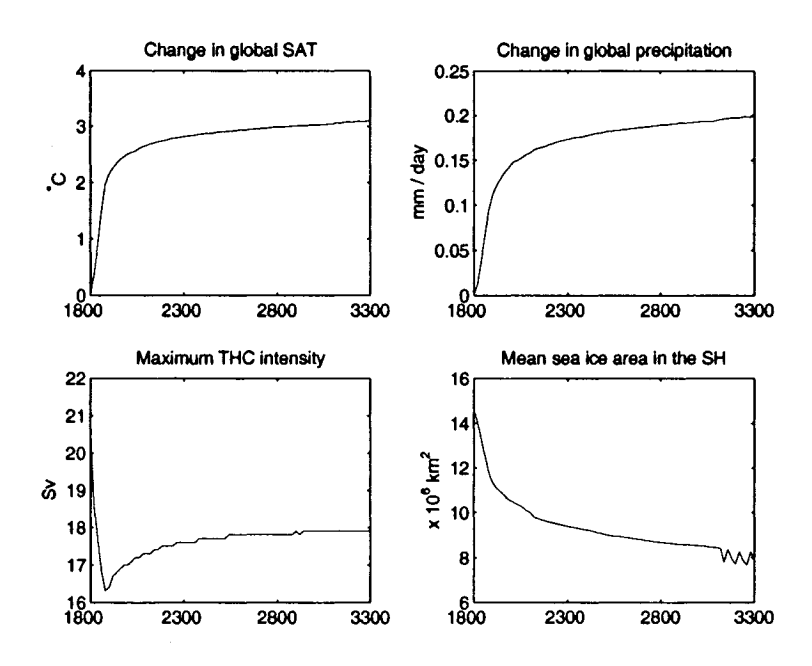


Figure 5.2: Time series of the changes, simulated by the MPM for the "equilibrium 2 x  $CO_2$ " run, in annual mean global SAT (top left) and precipitation (top right). Time series of the evolution of the maximum THC intensity (bottom left) and mean sea ice area in the Southern Hemisphere (bottom right) for the same run.

From Figure 5.2 (top left panel), we observe that, for the "equilibrium 2 x  $CO_2$ " run, the global SAT increases rapidly by 1.8°C during the first 70 years, and then increases more slowly before finally reaching a plateau of 3.1°C (2.9°C for the earlier version of the MPM) after 1500 years. This increase lies right in the middle of the range of 1.5°C to 4.5°C obtained by a number of GCMs for a  $CO_2$  doubling (Le Treut and McAvaney, 2000). We note that this increase also lies in the range of 1.4 and 5.8°C simulated over the period 1990-2100 by a number of GCMs using the  $CO_2$ 

scenarios from the SRES (Houghton *et al.*, 2001). Like the SAT, the precipitation also shows an increase, by an amount of 6 % after 1500 years (Figure 5.2, top right panel).

The lower left panel of Figure 5.2 also shows a strong reduction of the maximum strength of the THC during the first 100 years (- 4 Sv) followed by a progressive increase. However, the THC intensity never goes back to its initial value but asymptotes to an equilibrium value that is 2.6 Sv lower than the initial value. This might be due to a reduction of the North Atlantic Deep Water (NADW) formation rate triggered by a decrease of the density of the high northern latitude surface waters. The latter is due to a warming of the high latitude surface waters caused by the general warming of the climate, as well as a freshening of these waters due to an enhanced freshwater flux (increased precipitation and runoff) into the ocean at high latitudes. The total decrease of the THC strength is quite a bit larger than that obtained with the old version of the MPM (Petoukhov et al., 2004b). Manabe et al. (1991) and Manabe and Stouffer (1994) also obtained a weaker THC by using the same  $CO_2$ scenario with a coupled atmosphere-ocean GCM. Finally, we observe in the MPM simulation an initial rapid decrease of the sea ice area in the Southern Hemisphere, followed by a slower decrease (Figure 5.2, lower right panel). The sea ice area reaches an equilibrium value that is 54 % lower than the initial value.

## 5.3.2 Global warming experiment with atmospheric $CO_2$ stabilized at a reduced level

Rahmstorf and Ganopolski (1999) studied global warming scenarios with an atmosphere - ocean - sea ice model of intermediate complexity. They ran the model for 1200 years, with a scenario assuming that  $CO_2$  concentration will peak at 1200 ppm in the  $22^{nd}$  century and then decline afterwards, because of the exhaustion of fossil

fuels. Their results showed a strong decline of the THC, caused by a direct thermal forcing. The surface water at the poles was warmed up and freshened. The North Atlantic deep water formation was then reduced, which slowed down the THC. Their results showed that the THC intensity finally recovered, but it never went back to its initial value.

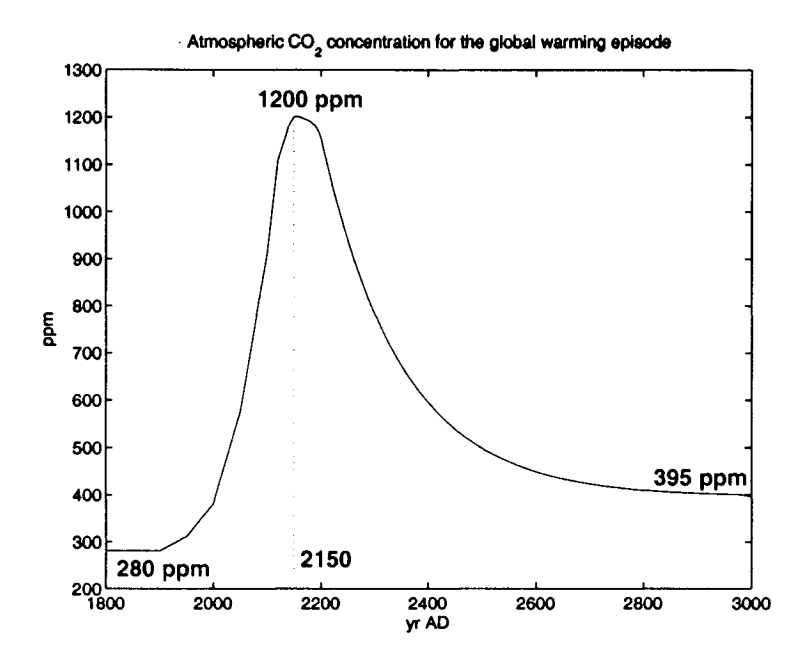


Figure 5.3: Atmospheric  $CO_2$  concentration for the global warming experiment, inspired by the one used by Rahmstorf and Ganopolski (1999).

The objective of this second short-term experiment is to determine whether the MPM, with its relatively low complexity (as compared to GCMs), is able to respond to a quick and intense warming radiative forcing. We ran the MPM for 1200 years, forced by the solar forcing calculated by Berger (1978). We used the same type of scenario for the  $CO_2$  concentration as used by Rahmstorf and Ganopolski (1999). As shown on Figure 5.3, the atmospheric  $CO_2$  concentration increases slowly from 1800 to 2000, and then rapidly reaches a maximum value of 1200 ppm in 2150. The increase of the  $CO_2$  concentration follows the IS92e IPCC scenario, i.e., the scenario with the fastest and largest increase of  $CO_2$  concentration. The  $CO_2$  concentration then slowly decreases, with an e-folding time of 150 years, and reaches an equilibrium

value of 395 ppm around year 3000. The pattern for the decrease of  $CO_2$  is based on the assumption that fossil fuel use will eventually cease, and that the ocean and the biosphere will slowly absorb the high level of  $CO_2$  remaining in the atmosphere.

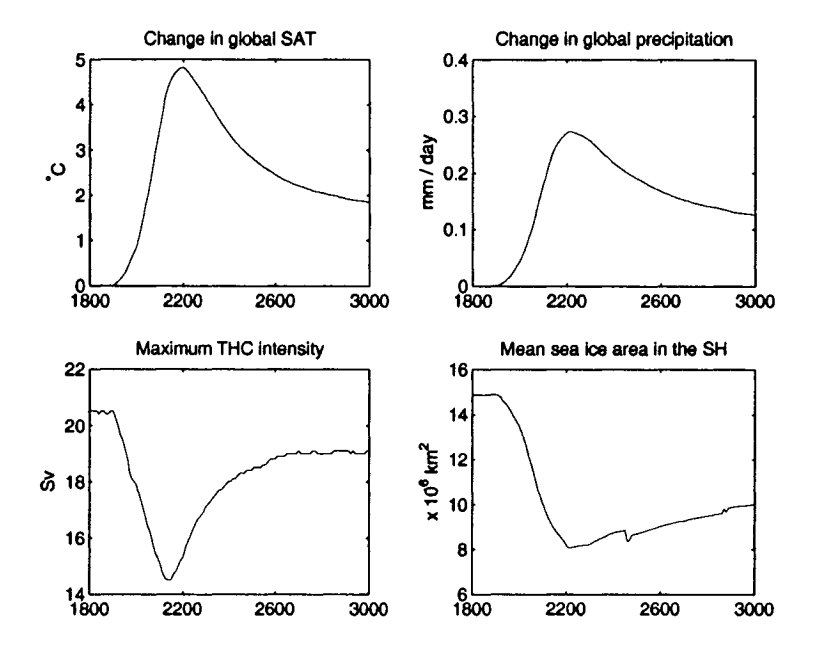


Figure 5.4: Time series of the changes in annual mean global SAT (top left) and precipitation (top right) simulated by the MPM for the global warming scenario, inspired by Rahmstorf and Ganopolski (1999). Time series of the evolution of the maximum THC intensity (bottom left) and mean sea ice area in the Southern Hemisphere (bottom right) for the same scenario.

From the two top panels of Figure 5.4, we note that the global SAT and precipitation changes follow quite closely the  $CO_2$  concentration scenario. They increase quite rapidly until 2200, with a maximum SAT change of 4.8°C and a maximum change in precipitation of 0.27 mm/day (i.e., an 8 % increase). The SAT and precipitation then decrease slowly and go back to values that are still greater than the pre-industrial values (by 1.8°C for the SAT, and by 0.12 mm/day for the global precipitation). From the two lower panels of Figure 5.4, we see that the maximum THC intensity and the mean sea ice area in the Southern Hemisphere first decrease rapidly until 2200 (by 6 Sv for the THC and 6.8 x  $10^6 \ km^2$  for the sea ice area). Then, the THC intensity and sea ice area rebound toward the starting values, but still remain lower than the pre-industrial values (by 1.4 Sv for the THC and by  $4.8 \times 10^6 \ km^2$  for the mean sea ice

area). Our results are quite similar to those obtained by Rahmstorf and Ganopolski (1999).

These short-term experiments (described in sections 5.3.1 and 5.3.2) show that the MPM is able to respond to rapid changes of the  $CO_2$  concentration. Despite its intermediate complexity, the MPM simulates well a warming of the climate (under a high  $CO_2$  concentration), whose peak temperature is in good agreement with the results of other EMICs and GCMs. We wish now to compare the modelled natural evolution of the climate and the modelled response of the climate to present and future rapid changes of the  $CO_2$  concentration induced by anthropogenic activities.

## 5.4 Long-term runs for the next 100 kyr

We next ran the model in order to simulate projections for the climate of the next 100 kyr, using a variety of  $CO_2$  scenarios. The solar forcing used was the one derived from Berger (1978); an example of this forcing for summer is shown on Figure 5.5.

### 5.4.1 Constant $CO_2$ concentration

In order to study the response of the climate to future changes in  $CO_2$ , we first ran simulations for the next 100 kyr with constant  $CO_2$  concentrations ranging from 210 to 370 ppm. Figure 5.6 shows the ice volume obtained over the Northern Hemisphere for atmospheric  $CO_2$  concentrations of 210, 230, 240, 250, 280, 310, 350 and 370 ppm.

Depending on the  $CO_2$  level, we see that there are three possible types of evolution for the ice volume: an imminent glacial inception, a glacial inception in 50 kyr, or no glacial inception. Mathematically speaking, the climate system passes through two thresholds for glaciation as the atmospheric  $CO_2$  is increased. For a concentration

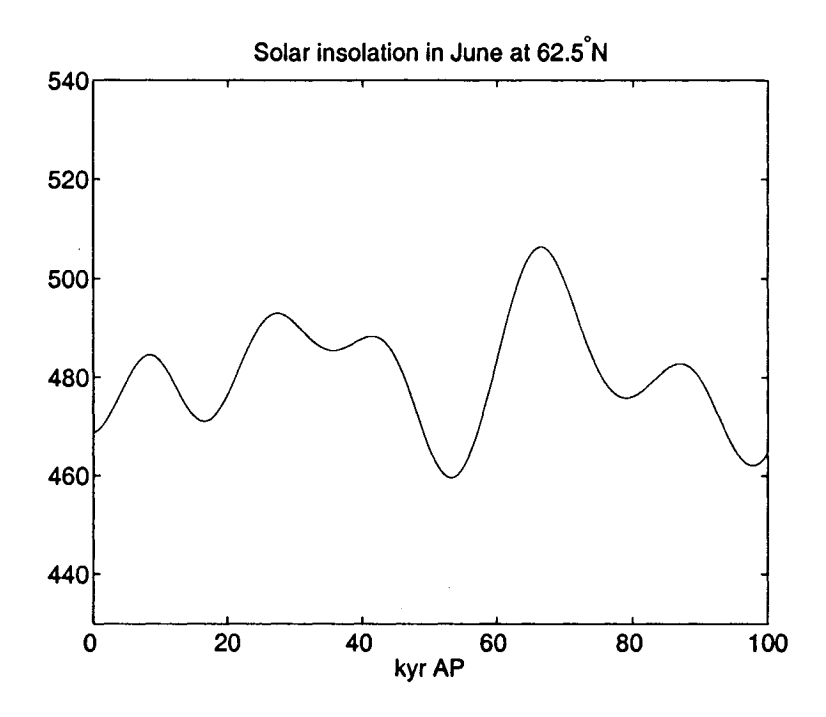


Figure 5.5: Solar insolation at a high northern latitude in summer, between 0 and 100 kyr AP, as calculated by Berger (1978).

of 210 ppm, the climate has already entered a glacial period and ice is present in northwestern North America. For the other  $CO_2$  concentrations smaller or equal to 240 ppm, the climate also enters into a glacial period fairly quickly. Ice starts to build up in the west of the high North American latitudes and then slowly expands eastward and southward. The Laurentide ice sheet, however, only starts to build up after 50 kyr. The ice volume then linearly increases from 50 kyr until 60 kyr AP, when it reaches a plateau, as seen on Figure 5.6. The ice sheets therefore tend to stabilize, with a total volume of 12.6 x  $10^6 \ km^3$ . For  $CO_2$  concentrations between 250 and 350 ppm, the MPM simulates a glacial inception in 50 kyr. Thus for some  $CO_2$  values between 240 and 250 ppm, the first threshold for glaciation is crossed. The increase of the ice volume, after this threshold is crossed, is  $CO_2$ -dependent. For a concentration of 250 ppm, we first observe a large increase of ice volume, and then a slower increase. However, for a concentration of 350 ppm, the MPM first simulates a slow buildup of ice sheets for about 25 kyr, which is followed by a more rapid buildup. The greater

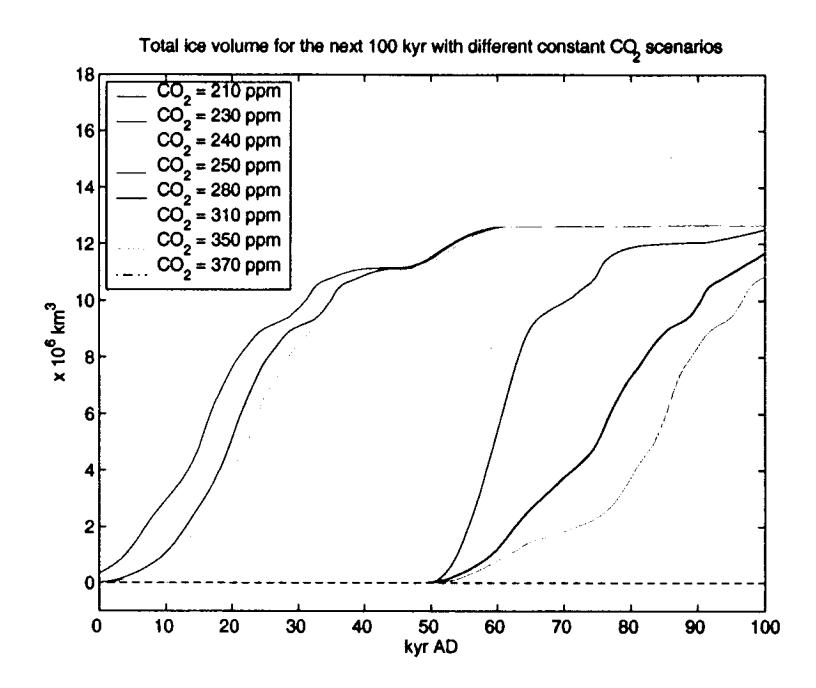


Figure 5.6: Ice volume simulated by the MPM over the North Hemisphere for the next 100 kyr, with constant  $CO_2$  scenarios ranging from 210 ppm (blue) to 370 ppm (dashed-dot black).

the  $CO_2$  concentration, the smaller the final volume of ice is  $(12.5 \times 10^6 \ km^3)$  for a concentration of 250 ppm versus  $10.9 \times 10^6 \ km^3$  for 350 ppm). The ice sheet first builds up over northwestern Canada and then expands eastward and southward. The appearance of the Laurentide ice sheet is also  $CO_2$ -dependent: the higher the  $CO_2$  concentration, the later the Laurentide ice sheet is formed. Finally, for concentrations greater or equal to 370 ppm, there is no glacial inception for the next 100 kyr. Thus there is a second threshold for glaciation between 350 and 370 ppm.

For the eight runs (with constant  $CO_2$  levels varying between 210 and 370 ppm) we observe an ice buildup over North America only, which has quite the same amplitude as that after the last glacial inception. On the other hand, there is no formation of ice sheets over Eurasia in the next 100 kyr. The Greenland ice volume varies very slightly, depending mainly on the variations of the solar insolation and the precipitation at high latitudes. The global SAT also varies slightly. The present-day value of the global SAT for a  $CO_2$  concentration of 370 ppm is only 0.3 °C higher than that for

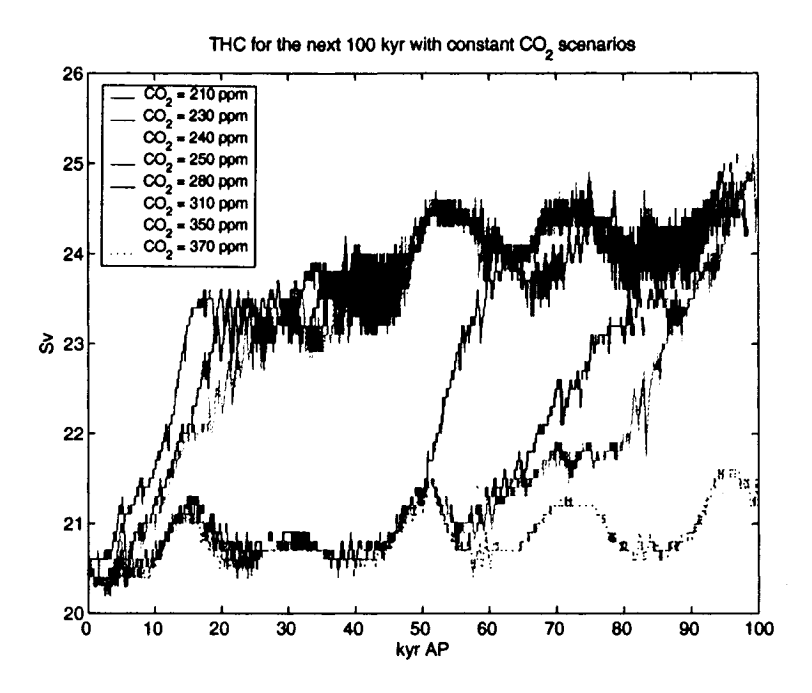


Figure 5.7: Maximum THC intensity simulated by the MPM for the next 100 kyr, with constant  $CO_2$  scenarios: 210 ppm (blue), 230 ppm (magenta), 240 ppm (cyan), 250 ppm (red), 280 ppm (black), 310 ppm (yellow), 350 ppm (green) and 370 ppm (dashed-dot black).

a concentration of 210 ppm. The evolution of the maximum THC strength for these eight different runs, as seen on Figure 5.7, shows an overall pattern similar to that for the ice volume, except that on each curve very small high-frequency fluctuations are superimposed. These might be linked to changes in Greenland ice volume and precipitation, that would modify the freshwater input at high latitudes. In the cases where a glacial inception occurs during the next 100 kyr, the total increase of the strength of the THC is around 4.1 Sv. It is also interesting to note, for the 370 ppm  $CO_2$  concentration, the existence of an approximate 20-kyr period oscillation in the THC strength, with peak-to-peak changes of about 1 Sv. One possible source for these oscillations may be the precessional signal in the orbital forcing. This signal seems also to be present for several of the other selected  $CO_2$  concentrations during periods when there is no large ice sheet growth. During the time of large ice sheet buildup, the THC seems to depend strongly on the ice volume evolution, as explained in section 2.1.4. At these times, the influence of the 20-kyr precessional signal has a

20-kyr precessional signal has a much smaller influence.

The natural evolution of the past  $CO_2$ , as observed in the Vostok ice core (Petit et al., 1999), shows that the  $CO_2$  concentration was around 280 ppm during preindustrial times. Moreover, due to anthropogenic activities, the value of the  $CO_2$  concentration is 373 ppm today and is expected to increase in the next one or two centuries. However, after this, with the depletion of fossil fuels, the  $CO_2$  level may drop below 370 ppm. It is thus plausible that the  $CO_2$  concentration will lie in the range 280 - 370 ppm during the future millennia. The imminent glacial inception, as simulated by the MPM for concentrations lower than 250 ppm, is thus not a possible scenario. Kukla et al. (1972) found a similar imminent glaciation because they were not considering the natural variations of  $CO_2$ , and were running models with an average  $CO_2$  concentration of 225 ppm.

To summarize, this set of model runs shows the existence of two thresholds for glaciation in the simulation of future climate with constant  $CO_2$ . For concentrations of 240 ppm and lower, the MPM simulates an imminent glaciation of the North Hemisphere. For concentrations between 250 and 350 ppm, the MPM simulates a glacial inception in  $\sim 50$  kyr. For concentrations of 370 ppm and higher, the MPM does not simulate any ice sheet buildup, at least for the next 100 kyr. For a concentration of 370 ppm, the MPM will actually simulate a glacial inception at around 130 kyr AP (not shown here). This glacial inception follows a drop of the high latitude summer insolation, which has a lower value (by  $4 \text{ W}/m^2$ ) than that at 50 kyr AP. These abrupt climate changes between ice-free and ice-covered northern latitudes are clear evidence of the strong non-linearity of the climate system.

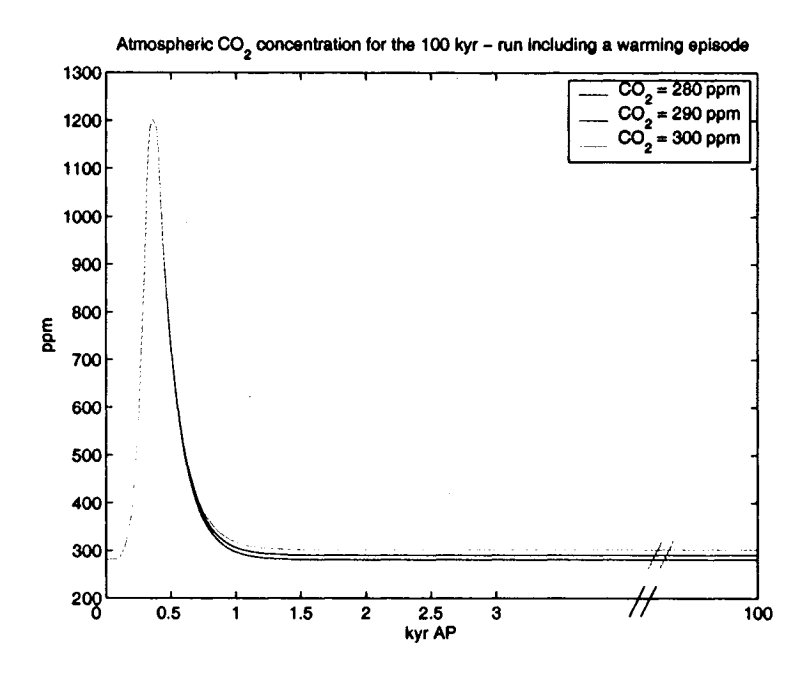


Figure 5.8: Atmospheric  $CO_2$  concentration for the global warming episode used in the 100 kyr experiment.

# 5.4.2 Constant $CO_2$ concentration after an episode of global warming

In order to study the impact of global warming on the long-term evolution of the climate, we ran 100-kyr simulations with a new scenario for the  $CO_2$  concentration. We included a global warming episode during the first 1200 years of the run, similar to that shown on Figure 5.3, and then we took the  $CO_2$  concentration to be a constant for the remaining years of the 100-kyr run. During the first 1200 years, the  $CO_2$  concentration quickly rises and falls, as seen on Figure 5.8. The concentration first increases during the first 350 years, up to a concentration of 1200 ppm. Then, it decreases slowly during the following 850 years, until it reaches a stable value. The  $CO_2$  concentration then remains at this stable value, which we call the "equilibrium value".

We ran a number of simulations with the  $CO_2$  "equilibrium value" varying between

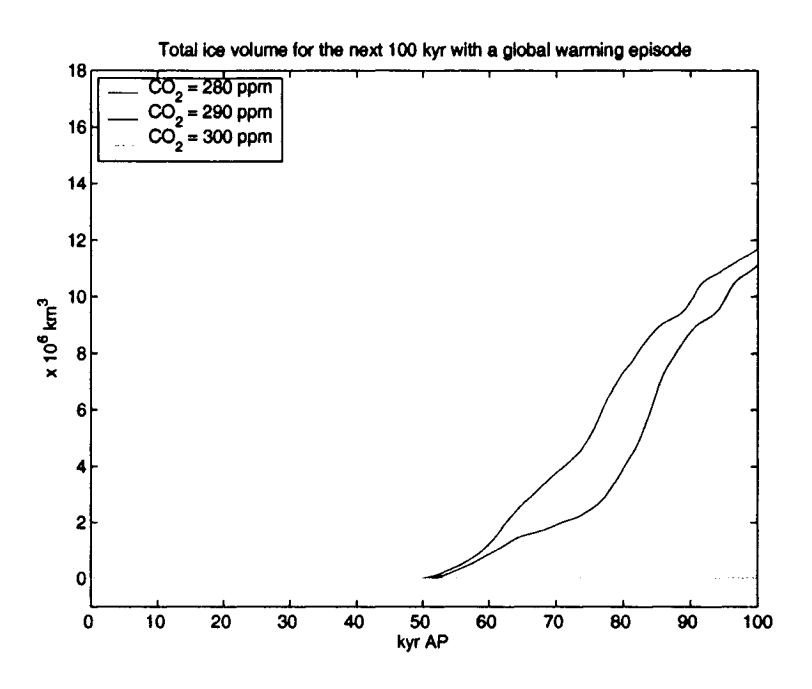


Figure 5.9: Ice volume over the North Hemisphere simulated by the MPM for the next 100 kyr, with a global warming episode followed by a constant  $CO_2$  scenario: 280 ppm (blue),290 ppm (red) and 300 ppm (green).

280 and 300 ppm. The evolution of the Northern Hemisphere ice volume is shown in Figure 5.9. Here again, we observe the existence of a threshold for glaciation. For  $CO_2$  concentrations of 290 ppm or lower, we observe a glacial inception at 50 kyr AP. For  $CO_2$  concentrations of 300 ppm or higher, the MPM does not simulate any glacial inception for the next 100 kyr. The threshold value is between 290 and 300 ppm and is therefore lower than the one obtained in section 5.4.1, which was between 350 and 370 ppm. Thus the addition of an initial global warming episode considerably lowers the  $CO_2$  level over which no glacial inception will occur.

As seen on Figure 5.10 (left panel), the maximum strength of the THC first rapidly decreases, in response to the  $CO_2$  increase and the subsequent general warming of the climate. The THC strength then rapidly increases until 1200 years AP, and then slowly decreases after this time. For a  $CO_2$  concentration of 280 ppm, the THC intensity returns finally to its initial value. This is not the case for the other  $CO_2$  concentrations. The THC strength at around 10 kyr AP, i.e., when it is stabilized

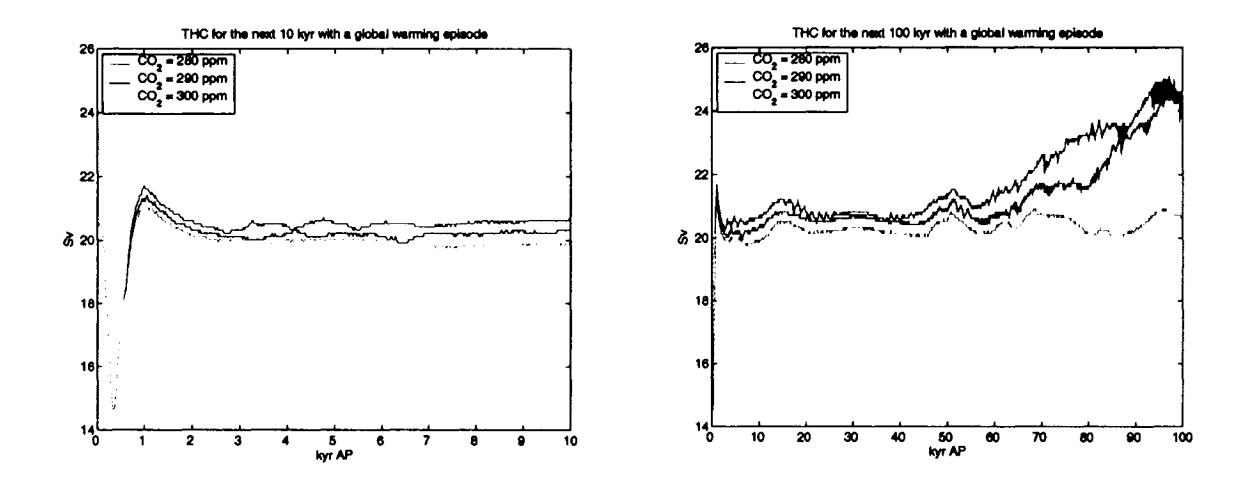


Figure 5.10: Maximum THC intensity simulated by the MPM with an initial global warming episode, followed by a constant  $CO_2$  concentration of 280 ppm (blue), 290 ppm (red) and 300 ppm (green). The left panel represents the first 10 kyr of the run, the right panel represents the total 100 kyr of the run.

after the global warming episode, is about 0.7 Sv (0.3 Sv) lower than the initial value, for a  $CO_2$  equilibrium value of 300 ppm (290 ppm). The evolution of the THC strength for the rest of the 100-kyr run (Figure 5.10, right panel) then follows the ice volume curve and increases after 50 kyr AP for  $CO_2$  levels of 280 and 290 ppm, due to the cooling of the climate generated by the buildup of ice sheets.

The addition of a global warming episode has thus changed the  $CO_2$  threshold over which no glacial inception occurs during the next 100 kyr. Figure 5.11 displays the maximum THC for the next 100 kyr, when the model is run under a constant  $CO_2$  concentration of 300 ppm, with a global warming episode included initially (blue curve) or not (red curve). For the first 3 kyr, the blue curve displays rapid changes in the THC strength due to the addition of the global warming episode. Then, and until 50 kyr AP, the THC strength has a similar pattern of evolution for both cases. However, the average value of the THC intensity is 0.7 Sv lower in the run including the global warming episode. After 50 kyr, the evolution of the THC strength is quite different. In the constant 300 ppm run, the THC strength increases after the glacial inception, up 3.8 Sv at the end of the run. In the run with the global warming episode, there is no glacial inception and the THC only weakly varies around its average value,

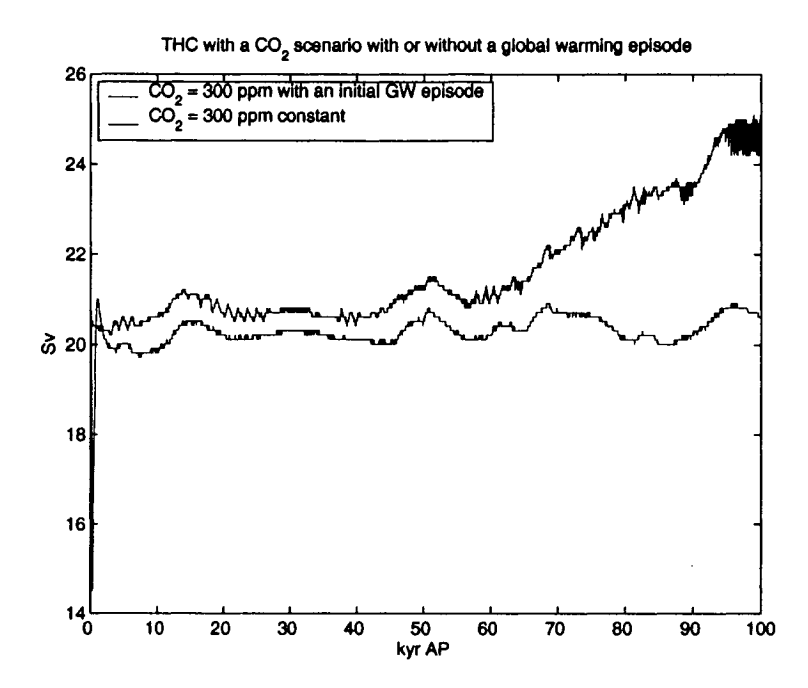


Figure 5.11: Maximum THC intensity simulated by the MPM for the next 100 kyr with a constant  $CO_2$  concentration of 300 ppm with an initial global warming episode (blue) or without (red).

depending on changes of the Greenland ice sheet and changes in high latitude upper ocean densities.

The addition of the rapid initial change in the  $CO_2$  forcing has triggered modifications of the early state of the climate system (THC strength, high latitude SAT). The response of the non-linear climate system to these small modifications might explain the difference in future climate evolutions. Furthermore, the ice volume growths simulated under concentrations of 280 and 290 ppm with the initial warming episode (Figure 5.9) are quite similar to the ones simulated under constant concentrations of 280 and 350 ppm, respectively, without the initial warming episode (as seen on Figure 5.6). The range of  $CO_2$  over which we observe a significantly different evolution of the climate is therefore reduced when the global warming episode is included in the simulations run with the MPM.

The Greenland ice volume varies only slightly over the next 100 kyr, as was ex-

plained in section 5.4.1. The MPM does not simulate any significant melting of the Greenland ice sheet. The MPM simulates only a slight increase of the Greenland ice volume, during the first 1200 years, due to increased precipitation at high latitudes. Our results are thus quite different from those of Loutre and Berger (2000a), who obtained an almost complete melting of the Greenland ice sheet for their long-term simulations including a global warming episode. However, Loutre (2003) has noted that one of the weaknesses of the LLN model was the too-frequent melting of the Greenland ice sheet during the warm interglacials. Finally, Letreguilly et al. (1991a) showed that with a 3-D ice sheet model, the Greenland ice sheet might be vulnerable to a climate warming, due to the presence of large ablation areas along the ice-sheet edges. The ice sheet would even disappear totally if a temperature increase of  $6^{\circ}C$ was sustained over 20 kyr, or 8°C sustained over 5 kyr. Using the scenario described earlier, with a  $CO_2$  "equilibrium value" of 300 ppm, the MPM only sustains a large increase of global temperature (up to 4.8 °C) over a few centuries. Once the SAT is stabilized, its value is only 0.5 °C higher than the initial value, and this does not trigger a melting of the Greenland ice sheet.

## Chapter 6

## Conclusions

## 6.1 Summary and conclusions

Simulations of the last and projections for the next glacial inceptions were run with the new version of the MPM, an Earth system model of intermediate complexity developed at McGill. The realistic insolation calculated by Berger (1978) was used to force the model. Since the MPM in these runs did not include a carbon cycle model, different prescribed scenarios of atmospheric  $CO_2$  concentration were also used as an external radiative forcing.

After the simulation of the last glacial inception by Wang and Mysak (2002), the MPM was significantly improved. A new solar energy disposition (SED) scheme was developed by Z.Wang et al. (2004), in order to simulate the shortwave radiative processes between the ground, the atmosphere and space in a more accurate way. An interactive vegetation component was then added to the model by Y.Wang et al. (2004). This allowed for the representation of the biogeophysical climate - vegetation feedback, i.e., the positive feedback between the surface air temperature, the

vegetation cover and the surface albedo.

With these new improvements, the MPM simulated a climate that was slightly too warm at 122 kyr BP. Some parameters were thus tuned in order to remove the warm bias and obtain the best configuration of the model to simulate the climate during the Eemian period. First, the ice sheet thickness was prescribed over Tibet. Secondly, the outgoing longwave radiation was slightly increased between 30 and 75°N, by decreasing the radiation trapped between the surface and the cloud layer. Thirdly, the cloud optical depth was increased, in order to increase the reflection of solar radiation by the atmosphere. Sensitivity studies (on vegetation albedos and the parameterization of the refreezing of liquid water on an ice sheet) were also run, in order to test the new version of the MPM.

In order to simulate the last glacial inception (LGI) and the subsequent ice volume growth, this version of the model was run between 122 and 80 kyr BP, and was forced by orbital-induced changes in the solar insolation and the observed Vostok-derived atmospheric  $CO_2$  concentration (Petit et al., 1999). The MPM simulated a glacial inception at around 119 kyr BP, followed by a large ice sheet growth over North America and a smaller one over Eurasia. The ice volume simulated over Eurasia was lower than the one simulated by Wang and Mysak (2002), mainly due to the addition of vast forests over northern Europe. Ice sheet buildup was thus affected by vegetation but not as a primary mechanism, since the MPM without the vegetation component was also able to simulate the LGI. Between 122 and 80 kyr BP, the Northern Hemisphere ice volume simulated by the "green" MPM was lower than that observed (Lambeck and Chappell, 2001). However, at 80 kyr BP, the simulated ice volume (19.9 x  $10^6 \ km^3$ ) was quite close to the observed value.

Ice sheets have slowly developed in the vicinity of the Laurentide, Cordilleran, Scandinavian and Siberian regions, and over Alsaka. They further expanded southward and longitudinally, to finally cover Alaska, northwestern Canada, northeastern

Canada, northwestern Europe and eastern Russia. Our results did not show any ice buildup over central North America, but a very thick and large ice sheet developed over Alaska. This thick ice simulated over Alaska might seem problematic. However, it is a common feature of ice sheet growth simulations in which spatial averages are used; the latter do not permit the resolution of spatial characteristics, as deep valleys and fjords in Alaska (Marshall, 2002). Since paleoclimatic records are quite rare for periods before the Last Glacial Maximum, it is difficult to determine if our ice sheet distribution is in agreement with what really happened. However, the simulation of a small ice sheet over northern Europe (compared to the large ice sheet obtained with the earlier version of the model) seems more in agreement with observed data.

We conclude, therefore, that the MPM is able to simulate the last glacial inception, when driven by realistic forcing. The ice volume simulated, however, is slightly too low, and displays an evolution that is too smooth. This is due to the limitations of the model, e.g., the coarse resolution, the absence of the Arctic and Antarctic regions, the sectorial averages which hide some regional aspects of the climate, the absence of thermodynamics in the ice sheet model and some missing or underestimated feedbacks. A study of changes in vegetation before and after the glacial inception would certainly add insight to the glacial inception process.

Short-term experiments for the future climate were then run in order to determine if the MPM was able to respond to a quick warming of the climate. Two scenarios of rapid increase of the atmospheric  $CO_2$  concentration were used: the first one represented a quick doubling of the  $CO_2$  concentration (Petoukhov et al., 2004b), and the second one was characterized by a strong increase of the  $CO_2$  level up to 1200 ppm, followed by a slow decrease over the next 1000 years. Both experiments showed that the MPM simulated a warm climate in response to the high level of  $CO_2$  and that the response lay in the range of other GCMs experiments (Houghton et al., 2001).

The model was finally run for the next 100 kyr, forced by realistic orbital insolation (Berger, 1978), in order to determine the date of occurrence of a possible glacial inception. The evolution of the summer insolation at high latitudes for the next 100 kyr is quite exceptional and displays only weak variations. The first drop in insolation occurs at around the present period. If this insolation drop is not low enough to trigger a glacial inception, there is a second drop in 50 kyr, which is even larger than the present-day one. Because of the absence of a carbon cycle in the MPM, we used different prescribed scenarios for the future evolution of the atmospheric  $CO_2$  concentration. We first ran the model forced by constant  $CO_2$  concentrations, between 210 and 370 ppm. Three possible cases appeared for the future evolution of the climate. A glacial inception was imminent for a  $CO_2$  concentration between 210 and 240 ppm, which was suggested by Kukla et al. (1972). For a CO<sub>2</sub> level between 250 and 350 ppm, the next glacial inception occurred in 50 kyr, which is similar to what was found by Loutre and Berger (2000a). For a  $CO_2$  concentration of 370 ppm or higher, no glacial inception occurred during the next 100 kyr. We then ran the same experiment, this time including a global warming episode during the first 1200 years. Here again, we observed a threshold for glaciation that depends on the  $CO_2$  concentration. For  $CO_2$  levels of 300 ppm or higher, a glacial inception would not occur in the next 100 kyr. The value of the threshold is different due to the modification of the climate system triggered by the addition of the global warming episode at the beginning of the run.

The conclusion of these experiments for future climate projections is that there exists thresholds in the atmospheric  $CO_2$  concentration, which determine the long-term evolution of the climate. The value of these thresholds varies depending on the initial conditions of the run. The amount of  $CO_2$  remaining in the atmosphere in the future will thus determine if a glacial inception will occur in the next 100 kyr. A further study of the evolution of certain atmospheric, oceanic and biospheric variables will be necessary to understand what determines these thresholds.

### 6.2 Concluding remarks

Since our experiments were carried out with a model of intermediate complexity, the "green" MPM, the results depend on the spatial resolution of the model. We could increase its resolution by using a longitude-latitude model instead of a sectorially averaged model, or by applying smaller scale models (such as nested models or models for individual glaciers or lake basins). This will improve our understanding of the small scale-phenomena that are important for interactions between the different components of the climate system. We could also increase the complexity of the MPM by increasing the number of components and important physical or biochemical processes, which are taken into account in the MPM, allowing for more internal feedbacks. However, this could considerably lengthen the computational time needed to run long-term simulations.

The MPM is being continuously improved. Some improvements could be very beneficial for the study of past and future abrupt climate changes. First of all, the addition of a global carbon cycle would allow the model to calculate the amount of  $CO_2$  which is absorbed or released by the biosphere and the ocean. If we know the amount of  $CO_2$  emitted by human activities, we can run the MPM to determine the  $CO_2$  remaining in the atmosphere. There will be no need anymore to prescribe scenarios for the future evolution of the  $CO_2$  concentration. The  $CO_2$  concentration will therefore be considered as a component of the climate system, and not an external forcing.

The addition of the Antarctic ice sheet and the Arctic region and the study of their impact on climate changes would also be of great interest. The Antarctic and Arctic regions will be added to the MPM by Dr Z. Wang. The northern and southern limits will therefore be 90°N and the MPM will be able to simulate ice sheet buildup at high latitudes. Later studies will allow us to determine the influence of these regions on the model behaviour. The ice sheet component of the MPM should also

be improved. Past climates have been affected by abrupt Heinrich Events (Heinrich, 1988), which were caused by freshwater pulses (due to massive iceberg calving or ice melting) and the subsequent modification of the ocean circulation. These events could occur again in the future, if there was large iceberg calving in Greenland. The absence of thermodynamics in the ice sheet model did not allow us to simulate these abrupt events. The consequences of replacing the isothermal ice sheet presently in the model with a polythermal ice sheet should therefore be studied.

Finally, we note that the addition of the vegetation component in the "green" MPM improved the simulation of the last glacial inception. However, only one vegetation - climate feedback was included in this version of the MPM, the biogeophysical feedback between the surface albedo and the vegetation cover. In order to represent the impact of a dynamic vegetation on the climate, in a more realistic way, two other feedbacks should be included: the vegetation - precipitation feedback, which would take into account the action of vegetation on the hydrological cycle, and the biogeochemical feedback, which would take into account the photosynthetic activity and the absorption and release of  $CO_2$  by the land biosphere.

## **Bibliography**

- ABER, J.D. (1992). Terrestrial ecosystems. In Trenberth, K., editor, *Climate System Modeling*, chapter 6, pages 173–200. Cambridge University Press.
- Andrews, J.T., Aksu, A., Kelly, M., Miller, R.G.H., Mode, W.N., and Mudie, P. (1985). Land/ocean correlations during the last interglacial/glacial transition, Baffin Bay, northwest North Atlantic: a review. *Quaternary Science Review*, 4:333-355.
- Andrews, J.T., Miller, R.G.H., Vincent, J.-S., and Shilts, W.W. (1986). Quaternary correlations in Arctic Canada. *Quaternary Science Review*, 5:243-250.
- Andrews, J.T. and Tedesco, K. (1992). Detrital carbonate-rich sediments, northwestern Labrador Sea: Implications for ice-sheet dynamics and iceberg rafting (Heinrich) events in the North Atlantic. *Geology*, 20:1087–1090.
- BARNOLA, J.M., RAYNAUD, D., LORIUS, C., AND BARKOV, N.I. (1999). Historical  $CO_2$  record from the Vostok ice core. In *Trends: A compendium of data on global change*. Carbon Dioxide Information Analysis Center, Oak Ridge National Laboratory, Department of Energy, U.S.
- BEERLING, D.J. AND WOODWARD, F.I. (2001). Vegetation and the terrestrial carbon cycle. Cambridge University Press, UK.
- BERGER, A. (1978). Long-term variations of daily insolation and Quaternary climatic changes. J. Atmos. Sci., 35:2362–2367.
- BERGER, A. (2001). The role of  $CO_2$ , sea level and vegetation during the Milankovitch-forced glacial-interglacial cycles. In BENGTSSON, L.O. AND HAMMER, C.U., editors, Geosphere-Biosphere interactions and climate, pages 119–146. Cambridge University Press, UK.
- BERGER, A., FICHEFET, T., GALLÉE, H., MARSIAT, I., TRICOT, C., AND VAN YPERSELE, J.-P. (1990). Physical interactions within a coupled climate model over the last glacial-interglacial cycle. *Trans. Roy. Soc. Edinburgh: Earth Sciences*, 81:357–369.

BERGER, A., GALLÉE, H., AND MELICE, J.L. (1991). The Earth's future climate at the astronomical time scale. In GOODESS, C.M. AND PALUTIKOV, J.P., editors, Future climate change and radioactive waste disposal, pages 148–165. (NIREX Safety Series NSS/R257, Climatic Research Unit, University of East Anglia, Norwich, UK).

- BERGER, A., GALLÉE, H., AND TRICOT, C. (1993b). Glaciation and deglaciation mechanisms in a coupled two-dimensional climate-ice sheet model. *J. Glaciol.*, 39(131):45–49.
- BERGER, A. AND LOUTRE, M.F. (1991). Insolation values for the climate of the last 10 million years. Quaternary Science Review, 10(4):297-317.
- BERGER, A. AND LOUTRE, M.F. (1996). Modelling the climate response to the astronomical and  $CO_2$  forcings. Comptes rendus de l'academie des sciences de Paris, t.323, serie IIa:1-16.
- BERGER, A., LOUTRE, M.F., AND GALLÉE, H. (1996). Sensitivity of the LLN 2-D climate model to the astronomical and  $CO_2$  forcing (from 200 kyr BP to 130 kyr AP). Scientific Report, 1996/1. Institut d'Astronomie et de Geophysique G. Lemaitre, Universite catholique de Louvain:pp. 1-49.
- BERGER, A., LOUTRE, M.F., AND TRICOT, C. (1993a). Insolation and Earth's orbital periods. J. Geophys. Res., 98(D6):10341-10362.
- BJORNSSON, H., MYSAK, L.A., AND SCHMIDT, G.A. (1997). Mixed boundary conditions versus coupling with an energy moisture balance model for a zonally averaged ocean climate model. *J. Climate*, 10:2412–2430.
- BOND, G., HEINRICH, H., BROECKER, W., LABEYRIE, L., MCMANUS, J., ANDREWS, J., HUON, S., JANTSCHIK, R., CLASEN, S., SIMET, C., TEDESCO, K., KLAS, M., BONANI, G., AND IVY, S. (1992). Evidence for massive discharges of icebergs into the North Atlantic ocean during the last glacial period. *Nature*, 360:245–249.
- Broecker, W.S. (1994). Massive iceberg discharges as triggers for global climate change. *Nature*, 372:421–424.
- BROECKER, W.S. (1998). The end of the present interglacial: how and when? *Quaternary Science Review*, 17:689-694.
- BROECKER, W.S. AND PENG, T.H. (1993). What caused the glacial to interglacial  $CO_2$  change? In Heimann, M., editor, *The global carbon cycle*, pages 95–115. NATO ASI Series, vol.15.
- Brovkin, V., Ganopolski, A., and Svirezhev, Y. (1997). A continuous climate-vegetation classification for use in climate-biosphere studies. *Ecological Modelling*, 101:251–261.

CLARK, P.U., CLAGUE, J.J., CURRY, B.B., DREIMANIS, A., HICOCK, S.R., MILLER, G.H., BERGER, G.W., EYLES, N., LAMOTHE, M., MILLER, B.B., MOTT, R.J., OLDALE, R.N., STEA, R.R., SZABO, J.P., THORLEIFSON, L.H., AND VINCENT, J.-S. (1993). Initiation and development of the Laurentide and Cordilleran ice sheets following the Last Interglaciation. *Quaternary Science Review*, 12:79–114.

- CLARK, P.U. AND POLLARD, D. (1998). Origin of the middle Pleistocene transition by ice sheet erosion of regolith. *Paleoceanography*, 13(1):1-9.
- CLAUSSEN, M., MYSAK, L.A., WEAVER, A.J., CRUCIFIX, M., FICHEFET, T., LOUTRE, M.F., WEBER, S.L., ALCAMO, J., ALEXEEV, V.A., BERGER, A., CALOV, R., GANOPOLSKI, A., GOOSSE, H., LOHMANN, G., LUNKEIT, F., MOKHOV, I.I., PETOUKHOV, V., STONE, P., AND WANG, Z. (2002). Earth system models of intermediate complexity: closing the gap in the spectrum of climate system models. *Climate Dynamics*, 18:579–586.
- CRUCIFIX, M. AND LOUTRE, M.F. (2002). Transient simulations over the last interglacial period (126-115 kyr BP): feedbacks and forcing analysis. *Climate Dynamics*, 19:417–433.
- CUFFEY, K.M. AND MARSHALL, S.J. (2000). Substantial contribution to sea-level rise during the last interglacial from the Greenland ice sheet. *Nature*, 404:591–594.
- CUFFEY, K.M. AND VIMEUX, F. (2001). Covariation of carbon dioxide and temperature from the Vostok ice core after deuterium-excess correction. *Nature*, 412:523–527.
- DE NOBLET, N.I., PRENTICE, C.I., JOUSSAUME, S., TEXIER, D., BOTTA, A., AND HAXELTINE, A. (1996). Possible role of atmosphere-biosphere interactions in triggering the last glaciation. *Geophys. Res. Lett.*, 23:3191–3194.
- DEBLONDE, G. AND PELTIER, W.R. (1991a). Simulations of continental ice sheet growth over the last glacial-interglacial cycle: experiments with a one-level seasonal energy balance model including realistic geography. J. Geophys. Res., 96:9189-9215.
- DEBLONDE, G. AND PELTIER, W.R. (1991b). A one-dimensional model of continental ice volume fluctuations through the Pleistocene: implications for the origin of the mid-Pleistocene climate transition. J. Climate, 4:318–344.
- DEBLONDE, G. AND PELTIER, W.R. (1993). Late Pleistocene ice age scenarios based on observational evidence. *J. Climate*, 6:709–727.
- DICKINSON, R.E., HENDERSON-SELLERS, A., AND KENNEDY, P.J. (1993). Biosphere Atmosphere Transfer sceme (BATS) for the NCAR Community Climate Model. ncar tn387+str. NCAR technical note, National Center for Atmospheric Research, Boulder, Colorado, Climate and Global Dynamic Division.

DICKINSON, R.E., HENDERSON-SELLERS, A., KENNEDY, P.J., AND WILSON, M.F. (1986). Biosphere Atmosphere Transfer scheme (BATS) for the NCAR Community Climate Model. ncar tn275+str. NCAR technical note, National Center for Atmospheric Research, Boulder, Colorado, Climate and Global Dynamic Division.

- FANNING, A.F. AND WEAVER, A.J. (1996). An atmospheric energy-moisture balance model: climatology, interpentadal climate change, and coupling to an ocean general circulation model. *J. Geophys. Res.*, 101:15111-15128.
- Gallimore, R.G. and Kutzbach, J.E. (1996). Role of orbitally induced changes in tundra area in the onset of glaciation. *Nature*, 381:503–505.
- GORDON, H.B. AND O'FARRELL, S.P. (1997). Transient climate change in the CSIRO coupled model with dynamic sea ice. *Mon. Wea. Rev.*, 125:875-907.
- GUPTA, S.K., RITCHEY, N.A., WILBER, A.C., AND WHITLOCK, C.H. (1999). A climatology of surface radiation budget derived from satellite data. *J. Climate*, 12:2691–2710.
- HARVEY, L.D.D. (1988). Development of a sea ice model for use in zonally averaged energy balance climate models. *J. Climate*, 1:1221–1238.
- HAYS, J.D., IMBRIE, J., AND SHACKLETON, N.J. (1976). Variations in the Earth's orbit: pacemaker of the ice ages. *Science*, 194:1121-1132.
- HEINRICH, H. (1988). Origin and consequences of cyclic ice rafting in the northeast Atlantic Ocean during the past 130,000 years. Quat. Res., 29:142-152.
- HELLERMAN, S. AND ROSENSTEIN, M. (1983). Normal monthly wind stress over the World Ocean with error estimates. J. Phys. Oceanogr., 13:1093-1104.
- HELMENS, K.F., RASANEN, M.E., JOHANSSON, P.W., JUNGNER, H., AND KORJONEN, K. (2000). The last interglacial-glacial cycle in NE Scandinavia: a nearly continuous record from Sokli (Finnish Lapland). *Quaternary Science Review*, 19:1605–1623.
- HIBLER, W.D. (1979). A dynamic thermodynamic sea ice model. J. Phys. Oceanogr., 9:815–846.
- HOUGHTON, J.T., DING, Y., GRIGGS, D.J., NOGUER, M., VAN DER LINDEN, P.J., DAI, X. AND. MASKELL, K., AND JOHNSON, C.A. (EDS). (2001). Climate change 2001: The scientific basis. contribution of working group I to the third assessment report of the intergovernmental panel on climate change. Cambridge University Press, Cambridge, United Kingdom and New York, USA, 881pp.
- HOWARD, W.R. (1997). A warm future in the past. Nature, 388:418-419.

IMBRIE, J., BERGER, A., BOYLE, E.A., CLEMENS, S.C., DUFFY, A., HOWARD, W.R., KUKLA, G., KUTZBACH, J., MARTINSON, D.G., McIntyre, A., Mix, A.C., Molfino, B., Morley, J.J., Peterson, L.C., Pisias, N.G., Prell, W.L., Raymo, M.E., Shackleton, N.J., and Toggweiler, J.R. (1993). On the structure and origin of major glaciation cycles. II. The 100,000-year cycle. *Paleoceanography*, 8:699–735.

- Imbrie, J., Boyle, E.A., Clemens, S.C., Duffy, A., Howard, W.R., Kukla, G., Kutzbach, J., Martinson, D.G., McIntyre, A., Mix, A.C., Molfino, B., Morley, J.J., Peterson, L.C., Pisias, N.G., Prell, W.L., Raymo, M.E., Shackleton, N.J., and Toggweiler, J.R. (1992). On the structure and origin of major glaciation cycles. I. Linear responses to Milankovitch forcing. *Paleoceanography*, 7(6):701–738.
- Janssens, I. and Huybrechts, P. (2000). The treatment of meltwater retention in mass-balance parameterisations of the greenland ice sheet. *Annals of Glaciology*, 31:133–140.
- JOHNSON, R.G. AND ANDREWS, T.J. (1979). Rapid ice-sheet growth and initiation of the last glaciation. *Quat. Res.*, 12:119–134.
- JOUZEL, J., BARKOV, N.I., BARNOLA, J.M., BENDER, M., CHAPELLAZ, J., GENTHON, C., KOTLYAKOV, V.M., LORIUS, C., PETIT, J.R., RAYNAUD, D., RAISBECK, G., RITZ, C., SOWERS, T., STIEVENARD, M., YIOU, F., AND YIOU, P. (1993). Vostok ice cores: extending the climatic records over the penultimate glacial period. *Nature*, 364(6436):407-412.
- KHODRI, M., LECLAINCHE, Y., RAMSTEIN, G., BRACONNOT, P., MARTI, O., AND CORTIJO, E. (2001). Simulating the amplification of orbital forcing by ocean feedbacks in the last glaciation. *Nature*, 410:570–574.
- Khodri, M., Ramstein, G., Paillard, D., Duplessy, J.-C., and Kageyama, M. (2003). Modelling the climate evolution from the last interglacial to the start of the last glaciation: the role of Arctic Ocean freshwater budget. *Geophys. Res. Lett.*, 30(12):1606, doi: 10.1029/2003GL017108.
- KUKLA, G.J., MATTHEWS, R.K., AND MITCHELL, M.J. (1972). Present interglacial: how and when will it end? *Quat. Res.*, 2:261-269.
- Kump, L.R. (2002). Reducing uncertainty about carbon dioxide as a climate driver. *Nature*, 419:188–190.
- LAMBECK, K. AND CHAPPELL, J. (2001). Sea level change through the last glacial cycle. *Science*, 292:679–686.
- LAMBECK, K., ESAT, T.M., AND POTTER, E.-K. (2002). Links between climate and sea levels for the past three million years. *Nature*, 419:199–206.

LE TREUT, H. AND MCAVANEY, B. (2000). A model intercomparison of equilibrium climate change in response to  $CO_2$  doubling. In *Notes du Pole de Modelisation de l'IPSL*, No.18. Institut Pierre Simon LaPlace, Paris, France.

- LEDLEY, T.S. (1991). The climatic response to meridional sea-ice transport. J. Climate, 4:147–163.
- LEDLEY, T.S. (1995). Summer solstice solar radiation, the 100 kyr ice age cycle and the next ice age. *Geophys. Res. Lett.*, 22:2745–2748.
- LETREGUILLY, A., HUYBRECHTS, P., AND REEH, N. (1991a). Steady-state characteristics of the Greenland ice sheet under different climates. *J. Glaciol.*, 37(125):149-157.
- LETREGUILLY, A., REEH, N., AND HUYBRECHTS, P. (1991b). The Greenland ice sheet through the last glacial-interglacial cycle. *Palaeogeogr.*, *Palaeoclimatol.*, *Palaeoecol.* (Global and Planet. Change Sect.), 90:385-394.
- LEVITUS, S. (1982). Climatological Atlas of the World Ocean. NOAA Professional Paper 13, 173pp.
- LI, Z. AND LEIGHTON, H.G. (1993). Global climatologies of solar radiation budgets at the surface and in the atmosphere from 5 years of ERBE data. *J. Geophys. Res.*, 98(D3):4919–4930.
- LOUTRE, M.F. (1995). Greenland ice sheet over the next 5000 years. *Geophys. Res. Lett.*, 22:783–786.
- LOUTRE, M.F. (2003). Clues from MIS 11 to predict the future climate a modelling point of view. *Earth Planet. Sci. Lett.*, 212:213-224.
- LOUTRE, M.F. AND BERGER, A. (2000a). Future climatic changes: Are we entering an exceptionally long interglacial? *Climatic change*, 46:61–90.
- LOUTRE, M.F. AND BERGER, A. (2000b). No glacial-interglacial cycle in the ice volume simulated under a constant astronomical forcing and a variable  $CO_2$ . Geophys. Res. Lett., 27(6):783–786.
- Manabe, S. (1969). Climate and the ocean circulation. I: The atmospheric circulation and the hydrology of the earth surface. *Mon. Wea. Rev.*, 97:739–774.
- MANABE, S., SPELMAN, M.J., AND BRYAN, K. (1991). Transient responses of a coupled ocean-atmosphere model to a gradual change of atmospheric  $CO_2$ . Part I: Annual mean response. J. Climate, 4:785–818.
- MANABE, S. AND STOUFFER, R.J. (1988). Two stable equilibria of a couple ocean-atmosphere model. J. Climate, 1:841-866.

Manabe, S. and Stouffer, R.J. (1994). Multiple-century response of a coupled ocean-atmosphere model to an increase of atmospheric carbon dioxide. *J. Climate*, 7:5–23.

- MANGERUD, J. (2004, in press). Ice sheet limits on Norway and the Norwegian continental shelf. Quaternary Glaciations Extent and Chronology. Vol. 1 Europe, Elsevier, Amsterdam.
- MARSHALL, S.J. (2002). Modelled nucleation centres of the Pleistocene ice sheets from an ice sheet model with subgrid topographic and glaciologic parameterizations. *Quaternary International*, 95-96:125-137.
- MARSHALL, S.J. AND CLARKE, G.K.C. (1997). A continuum mixture model of ice stream thermomechanics in the Laurentide Ice Sheet, 1. Theory. *J. Geophys. Res.*, 102:20599–20613.
- McManus, J.F., Oppo, D.W., and Cullen, J.L. (1999). A 0.5-million-year record of millenial scale climate variability in the North Atlantic. *Science*, 283:971–975.
- MEISSNER, K.J., WEAVER, A.J., MATTHEWS, H.D., AND COX, P.M. (2003). The role of land surface dynamics in glacial inception: a study with the UVic Earth System Model. *Climate Dynamics*, 21:515–537.
- MILANKOVITCH, M.M. (1941). Canon of insolation and the ice-age problem. Koniglich Serbische Akad., Belgrade, Yugoslavia.
- OERLEMANS, J. AND VAN DER VEEN, C.J. (1984). *Ice sheets and climate*. Reidel publishing, Dordrecht, p.217.
- Oppo, D.W., McManus, J.F., and Cullen, J.L. (1998). Abrupt climate events 500,000 to 340,000 years ago: Evidence from subpolar North Atlantic sediments. *Science*, 279:1335–1338.
- PELTIER, W.R. (1994). Ice age paleotopography. Science, 265:195–201.
- Petit, J.R., Jouzel, J., Raynaud, D., Barkov, N.I., Barnola, J.M., Basile, I., Benders, M., Chapellaz, J., Davis, M., Delaygue, G., Delmotte, M., Kotlyakov, V.M., Legrand, M., Lipenkov, V.Y., Lorius, C., Pepin, L., Ritz, C., Saltzman, E., and Stievenard, M. (1999). Climate and atmospheric history of the past 420,000 years from the Vostok ice core, Antarctica. *Nature*, 399:429–436.
- PETOUKHOV, V., CLAUSSEN, M., BERGER, A., CRUCIFIX, M., EBY, M., ELISEEV, A., FICHEFET, T., GANOPOLSKI, A., GOOSSE, H., KAMENKOVICH, I., MOKHOV, I., MONTOYA, M., MYSAK, L.A., SOKOLOV, A., STONE, P.,

Wang, Z., and Weaver, A.J. (2004b). EMIC Intercomparison Project (EMIP- $CO_2$ ): Comparative analysis of EMIC simulations of current climate and equilibrium and transient responses to atmospheric  $CO_2$  doubling. Part II: equilibrium and transient responses to  $CO_2$  doubling. submitted to Climate Dynamics.

- PINCUS, R., SZCZODRAK, M., Gu, J., AND AUSTIN, P. (1995). Uncertainty in cloud optical depth estimates made from satellite radiance measurements. *J. Climate*, 8:1453–1462.
- RAHMSTORF, S. AND GANOPOLSKI, A. (1999). Long-term global warming scenarios computed with an efficient coupled climate model. *Climatic Change*, 43:353–367.
- RUDDIMAN, W.F. (2003a). Orbital insolation, ice volume and greenhouse gases. *Quaternary Science Review*, 22:1597–1629.
- RUDDIMAN, W.F. (2003b). The anthropogenic greenhouse era began thousands of years ago. *Climatic Change*, 61:261–293.
- RUDDIMAN, W.F. AND THOMSON, J.S. (2001). The case for human causes of increased atmospheric  $CH_4$  over the last 500 years. Quaternary Science Review, 20:1769–1777.
- SALTZMANN, B., MAASCH, K.A., AND VERBITSKY, M.Y. (1993). Possible effects of anthropogenically-increased  $CO_2$  on the dynamics of climate: implications for ice age cycles. *Geophys. Res. Lett.*, 20:1051–1054.
- SCHMIDT, G.A. AND MYSAK, L.A. (1996). The stability of a zonally averaged thermohaline circulation model. *Tellus*, 48A:158–178.
- SEMTNER, A.J. (1976). A model for the thermodynamic growth of sea ice in numerical investigations of the climate. J. Phys. Oceanogr., 6:379-389.
- STOCKER, T.F. AND KNUTTI, R. (2003). Do simplified climate models have any useful skill? *CLIVAR Exchanges*, 8 (No 1):7–10.
- STOCKER, T.F., WRIGHT, D.J., AND MYSAK, L.A. (1992). A zonally averaged, coupled ocean-atmosphere model for paleoclimate studies. *J. Climate*, 5:773–797.
- Stommel, H. (1961). Thermohaline convection with two stable regimes of flow. *Tellus*, 13:224–230.
- Svendsen, J.I., Astakhov, V.I., Bolshiyanov, D.Y., Dowdeswell, J.A., Gataullin, V., Hjort, C., Hubberten, H., Larsen, E., Mangerud, J., Moller, P., Saarnisto, M., and Siegert, M.J. (1999). Maximum extent of the Eurasian ice sheets in the Barents and Kara Sea region during the Weichselian. *Boreas*, 28:234–242.

TARASOV, L. AND PELTIER, W.R. (1997). Termination of the 100 kyr ice age cycle. J. Geophys. Res., 102:21665-21693.

- TARASOV, L. AND PELTIER, W.R. (1999). The impact of thermomechanical ice-sheet coupling on a model of the 100 kyr ice age cycle. *J. Geophys. Res.*, 104:9517–9545.
- TARASOV, L. AND PELTIER, W.R. (2004). A geophysically constrained large ensemble analysis of the deglacial history of the North American ice-sheet complex. *Quaternary Science Review*, 23(3-4):359–388.
- THOMPSON, S.L. AND WARREN, S.G. (1982). Parameterization of outgoing infrared radiation derived from detailed radiative calculations. *J. Atmos. Sci.*, 39:2667–2680.
- VETTORETTI, G. AND PELTIER, W.R. (2003a). Post-Eemian glacial inception. Part I: the impact of summer seasonal temperature bias. *J. Climate*, 16:889–911.
- VETTORETTI, G. AND PELTIER, W.R. (2003b). Post-Eemian glacial inception. Part II: elements of a cryospheric moisture pump. *J. Climate*, 16:912–927.
- VETTORETTI, G. AND PELTIER, W.R. (2004). Sensitivity of glacial inception to orbital and greenhouse gas climate forcing. *Quaternary Science Review*, 23(3-4):499–519.
- VISSER, K., THUNNEL, R., AND STOTT, L. (2003). Magnitude and timing of temperature change in the Indo-Pacific warm pool during deglaciation. *Nature*, 421:152–155.
- WANG, Z. AND MYSAK, L.A. (2000). A simple coupled atmosphere-ocean-sea iceland surface model for climate and paleoclimate studies. *J. Climate*, 13:1150–1172.
- WANG, Z. AND MYSAK, L.A. (2001). Ice sheet Thermohaline circulation interactions in a climate model of intermediate complexity. *Journal of Oceanography*, 57:481-494.
- Wang, Z. and Mysak, L.A. (2002). Simulation of the last glacial inception and rapid ice sheet growth in the McGill Paleoclimate Model. *Geophys. Res. Lett.*, 29(23):2102, doi: 10.1029/2002GL015120.
- Wang, Z., Mysak, L.A., and McManus, J.F. (2002). Response of the thermohaline circulation to cold climates. *Paleoceanography*, 17:NO.1, 10.1029/2000PA000587.
- WRIGHT, D.G. (1997). An equation of state for use in ocean models: Eckart's formula revisited. J. Atmos. Oceanic Technol., 14:735-740.

WRIGHT, D.G. AND STOCKER, T.F. (1991). A zonally averaged ocean model for the thermohaline circulation. I: Model development and flow dynamics. *J. Phys. Oceanogr.*, 21:1713–1724.

- Y.Wang, Mysak, L.A., and Brovkin, V. (2004). The greening of the McGill Paleoclimate Model. Part I: Improved land surface scheme with vegetation dynamics. *Climate Dynamics*, submitted.
- ZHANG, Y.-C., ROSSOW, W.B., AND LACIS, A.A. (1995). Calculation of surface and top of atmosphere radiative fluxes from physical quantities based in ISCCP data sets. 1. Method and sensitivity to input data uncertainties. *J. Geophys. Res.*, 100:1149–1165.
- Z.Wang, Hu, R.-M., Mysak, L.A., Blanchet, J.-P., and Feng, J. (2004). A parameterization of solar energy disposition in the climate system. *Atmosphere-Ocean*, in press.